https://doi.org/10.5194/egusphere-2026-3000
Preprint. Discussion started: 18 June 2026

EarthCARE reveals details on the role of rain in closed-to-open cell transitions

Johanna Mayer[1], Daniele Gasbarra[1], Robin J. Hogan[2], Edward Malina[1], Shannon L. Mason[2], and Blanka Piskala Gvozdikova[1]

[1]European Space Agency - ESRIN, Frascati, Italy
[2]European Centre for Medium-Range Weather Forecasts, Reading, United Kingdom

Correspondence: Johanna Mayer (johanna.mayer@esa.int)

Abstract. The mesoscale organisation of marine stratocumulus clouds into closed and open cells strongly affects cloud albedo and thus their cooling effect on climate, yet the processes governing transitions between these regimes remain incompletely understood. The EarthCARE satellite provides collocated observations of cloud mesoscale structure from the Multi-Spectral Imager (MSI) together with vertically resolved cloud and precipitation measurements from the Atmospheric Lidar (ATLID) and Cloud Profiling Radar (CPR), enabling detailed characterization of stratocumulus cloud microphysics. We apply a convolutional neural network to MSI scenes to identify closed and open cells and relate these classifications to EarthCARE microphysical retrievals from the synergy of ATLID, CPR, and MSI. Open cells exhibit substantially lower droplet number concentrations (N_d), greater variability in liquid water path (LWP) and droplet sizes (r_e), and more frequent and heavier precipitation, although light drizzle is also common in closed cells. To investigate closed-to-open cell transitions, we combine EarthCARE overpasses with GOES/ABI geostationary imagery and ERA5-driven trajectories to track cloud scenes and determine transition timing. This combined approach allows us to reconstruct the temporal evolution of cloud properties around transitions. We find that LWP and rain amounts increase in closed cells up to $\tilde{2}5$ hours before transitions, followed by decreasing N_d and increasing r_e, while cloud vertical structure remains largely unchanged. These findings support a precipitation-linked transition pathway, potentially triggered by enhanced boundary-layer moisture and amplified by aerosol scavenging–rain feedback. This new observational evidence advances our understanding of stratocumulus breakup with implications for the cooling effect of these clouds.

1 Introduction

Marine stratocumulus clouds play a pivotal role in Earth's climate system, reflecting much of the incoming solar radiation back to space. An important aspect of stratocumulus clouds is their mesoscale organization, i.e. cloud pattern organization on horizontal scales of the order of kilometres to 100 km. A prominent manifestation of this mesoscale organization is the occurrence of *closed-cell* and *open-cell* stratocumulus (Wood and Hartmann, 2006; Wood et al., 2008; Muhlbauer et al., 2014; Koren et al., 2017; Mohrmann et al., 2021). Closed cells are generally associated with high cloud fraction and high albedo, whereas open cells exhibit broken cloud fields with reduced cloud fraction and lower albedo (Wood and Hartmann, 2006;

https://doi.org/10.5194/egusphere-2026-3000
Preprint. Discussion started: 18 June 2026

McCoy et al., 2017; Danker et al., 2022; McCoy et al., 2023). A transition from closed to open cells usually leads to a drop in cloud albedo and consequently the clouds' cooling effect. As a result, uncertainties in the representation of stratocumulus clouds remain a major contributor to the spread in climate sensitivity and cloud feedbacks in climate models (Bony and Dufresne, 2005; Ceppi et al., 2017; on Climate Change , IPCC). Understanding the processes that lead to mesoscale structure changes and the break-up of closed stratocumulus decks is especially pressing in light of new findings that a decrease in cloud fraction of low-level clouds is the main reason for the increasing positive energy imbalance of the Earth (Loeb et al., 2024).

Despite substantial progress, the processes governing transitions between closed and open cells remain incompletely understood. Several mechanisms have been proposed and intensively investigated, including aerosol-cloud-precipitation interactions, cold-pool dynamics, cloud-top entrainment and instability, and the influence of surface forcing and large-scale meteorology (Savic-Jovcic and Stevens, 2008; Wang and Feingold, 2009a, b; Feingold et al., 2010; Yamaguchi and Feingold, 2015; Jensen et al., 2021; Chandrakar et al., 2022; McCoy et al., 2023). In particular, precipitation has long been hypothesized to play a key role in promoting open-cell conditions (Stevens et al., 2005; Wood et al., 2008). Large-Eddy Simulations (LES) show that in simulations with low aerosol concentrations and consequently heavier rain, open cells are the preferred state (Savic-Jovcic and Stevens, 2008; Wang and Feingold, 2009a; Berner et al., 2013; Yamaguchi and Feingold, 2015; Chandrakar et al., 2022; Hoffmann et al., 2023). The proposed physical mechanism is the cold-pool convergence hypothesis: precipitation generates evaporatively cooled downdrafts whose cold, moist outflows spread near the surface. Collisions between these outflows can trigger updrafts that reorganize the cloud field into open cells (Savic-Jovcic and Stevens, 2008; Yamaguchi and Feingold, 2015).

Observational studies from multiple field campaigns and case studies report stronger drizzle and reduced aerosol concentrations in open-cell or pocket-of-open-cells (POC) conditions (Stevens et al., 2005; Sharon et al., 2006; Jensen et al., 2021). Satellite studies have provided evidence that open cells typically consist of fewer, larger cloud droplets and that these cloud structures are associated with stronger winds and lower inversion strength (e.g., Muhlbauer et al., 2014; McCoy et al., 2017; Mohrmann et al., 2021). Recent work has also adopted Lagrangian frameworks to track cloud scenes through time using wind trajectories combined with imagery from polar-orbiting (Eastman et al., 2022) and geostationary satellites (Smalley et al., 2022). These approaches have strengthened evidence that precipitation is closely linked to the closed-to-open transition, consistent with the cold-pool convergence hypotheses (Eastman et al., 2022; Smalley et al., 2022).

However, progress has been limited by observational constraints. Passive sensors infer precipitation indirectly and often struggle with light drizzle, large footprints, and limited ability to resolve the vertical distribution of hydrometeors. Additionally, precipitation retrievals are frequently not collocated with the cloud microphysical retrievals used to infer droplet number concentration or effective radius, complicating process interpretation along a Lagrangian track (Smalley et al., 2022). At the same time, other studies have reported that drizzle differences between open and closed cells may be modest in some conditions, suggesting that precipitation-related thermodynamic feedbacks are not the sole factor controlling mesoscale organization (Wood et al., 2011; Terai et al., 2014; Yamaguchi and Feingold, 2015). Further, while aerosol depletion within POCs is frequently observed and may promote precipitation by reducing droplet number concentrations, the causal sequence between

https://doi.org/10.5194/egusphere-2026-3000
Preprint. Discussion started: 18 June 2026

precipitation enhancement, aerosol scavenging, and mesoscale breakup remains debated (Wood et al., 2008; Smalley et al., 2022; Eastman et al., 2022; Chandrakar et al., 2022).

The Earth Cloud, Aerosol and Radiation Explorer (EarthCARE), launched in May 2024 (Eisinger et al., 2024), provides a new opportunity to study stratocumulus clouds with unprecedented detail and address these gaps. Firstly, EarthCARE carries both active (Atmospheric Lidar, ATLID, and Cloud Profiling Radar, CPR) and passive (Multi-Spectral Imager, MSI) sensors on board. This combination provides collocated measurements of mesoscale structure and vertically resolved information of aerosol, cloud and rain properties. Secondly, the EarthCARE CPR overcomes major limitations of earlier missions such as CloudSat by providing enhanced sensitivity, finer vertical and horizontal resolution, and greatly reduced surface-clutter contamination. Using the first year of CPR observations, Xu et al. (2025) show that surface clutter is effectively suppressed above approximately 0.5 km and that CPR detects substantially more stratocumulus than CloudSat's radar instrument in key subtropical regions, and improved identification of light precipitation occurrence. Furthermore, as the first spaceborne Doppler radar, EarthCARE's CPR provides vertical velocity estimates tightly linked to raindrop fall speeds. Combining reflectivity and Doppler velocity yields better constraints on raindrop sizes and improves retrievals of rain rate and liquid water content compared to single-frequency radars (Mason et al., 2023). These advances enable more reliable detection and characterization of shallow marine clouds and drizzle close to the ocean surface, a regime that was challenging before. This capability is particularly important for stratocumulus transitions, where drizzle and its subcloud evaporation are thought to be important drivers for cloud breakup (Wood et al., 2008; Yamaguchi and Feingold, 2015; Cadeddu et al., 2020; Smalley et al., 2022; Eastman et al., 2022).

While EarthCARE provides detailed instantaneous information, it is still a polar-orbiting platform and therefore samples any given region infrequently, with a revisit time of about 25 days for the active instruments. Therefore, to study transitions, it is best to combine EarthCARE snapshots with the continuous temporal coverage of geostationary satellites. Geostationary imagery can track mesoscale cloud organization and identify the timing of transitions, while EarthCARE provides a physically rich characterization of the cloud and precipitation column during overpass.

In this study, we exploit this combination of EarthCARE and geostationary satellites to investigate closed and open cell stratocumulus organization and transitions in the subtropics. We address two main research questions:

1. We quantify differences in cloud and precipitation properties between open and closed cells from the perspective of EarthCARE, taking advantage of the satellite's improved capabilities to measure these quantities and a convolutional neural network (CNN) to classify clouds into different mesoscale structures.

2. We examine how these properties evolve in the hours leading up to and following a closed-to-open cell transition. To this end we use a Lagrangian perspective, combining EarthCARE with geostationary measurements of the Geostationary Operational Environmental Satellite (GOES) along wind trajectories. We use this information to assess candidate transition mechanisms, with a focus on the role of precipitation and its associated dynamical feedbacks.

The the paper is structured as follows. Section 2 describes the datasets and methodology, including the EarthCARE cloud and precipitation retrievals, the CNN used for mesoscale structure classification and the tracking framework. Section 3.1 presents

https://doi.org/10.5194/egusphere-2026-3000
Preprint. Discussion started: 18 June 2026

the EarthCARE-based contrasts between open and closed cellular regimes. Section 3.2 analyses the time evolution of cloud and rain properties relative to transition time. Section 4 discusses uncertainties, and assesses implications for transition mechanisms and regional generality.

2 Data and Methods

EarthCARE observations used in this study are taken from product baseline BA, covering August 2024 to November 2025. Later observations are available but belong to a subsequent processing baseline and are not included here for consistency. The study domain comprises four well-established subtropical stratocumulus regions: the Southeast Pacific (SEP), Northeast Pacific (NEP), Southeast Atlantic (SEA), and Northeast Atlantic (NEA), each with an extent of $20° \times 20°$ longitude and latitude (see Fig. 1). These regions are frequently used for evaluating closed and open cell stratocumulus clouds (Wood and Hartmann, 2006; Wood et al., 2008; Muhlbauer et al., 2014; Mohrmann et al., 2021; Fons et al., 2024).

We construct a dataset containing EarthCARE observations over the four stratocumulus regions, combining information on cloud and rain properties, with mesoscale cloud-structure characteristics. A CNN is used to classify cloud scenes into mesoscale structure classes, most notably closed and open cells. For the SEP region, we additionally incorporate GOES geostationary data to introduce a temporal dimension, enabling analysis of transitions between closed- and open-cell regimes. The SEP region was chosen out of the four stratocumulus regions for this second part of the study, because it contains the largest number of open cells (see Fig. 1).

In the following subsections, we describe the data sources and processing steps in detail, including the three EarthCARE data products used, the GOES imagery, the wind trajectories, and the CNN-based cloud-scene classification.

2.1 EarthCARE ACM-CAP for detailed cloud and rain observations

The ACM-CAP product provides a synergistic retrieval of clouds, aerosols, and precipitation from the combination of EarthCARE's active and passive instruments, ATLID, CPR and MSI. It uses the CAPTIVATE optimal estimation retrieval framework and delivers a comprehensive set of products including profiles of liquid clouds and rain (Mason et al., 2023). ACM-CAP is unique in that it provides a unified retrieval of all hydrometeors and aerosols. This has the advantage of facilitating retrievals even in complex atmospheric situations (Mason et al., 2023) and ensures vertical consistency for hydrometeor properties. The products are provided at 1 km horizontal resolution along track and 100 m vertical resolution.

To focus on stratocumulus regimes, we retain only single-layer, low-level clouds by selecting clouds with cloud-top height (CTH) < 3 km, consistent with the typical depth of marine stratocumulus decks (Leon et al., 2008; Muhlbauer et al., 2014; Xu et al., 2025). Only clouds over the ocean are considered.

Cloud geometric properties (CTH and cloud-base height, CBH) are extracted from the ACM-CAP liquid cloud mask ("liquid_classification"). For cloud microphysics, we use ACM-CAP retrievals of liquid water content, cloud droplet effective radius (r_e), droplet number concentration (N_d), rain water content, and rain median volume diameter (D_0). In this study, we focus on column-integrated or averaged values: Liquid water content, and rain water content are vertically integrated to obtain liquid

https://doi.org/10.5194/egusphere-2026-3000
Preprint. Discussion started: 18 June 2026

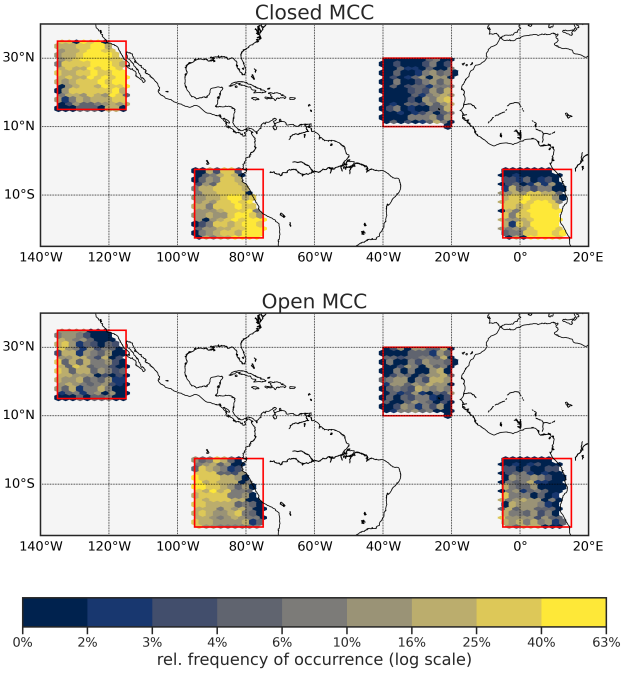

Figure 1. Geographic distribution of closed and open cells in four stratocumulus regions in terms of relative frequency of occurrence. Relative frequency of occurrence is computed as the fraction of occurrences of closed or open cells, as detected by the CNN applied to MSI, to the total number of all mesoscale cloud structure occurrences, expressed as percentage.

water path (LWP) and rain water path (RWP). The r_e and D_0 values are averaged per profile, and N_d is for liquid clouds already reported as a profile-constant value, following the ACM-CAP retrieval design (Mason et al., 2023). Error estimates from ACM-CAP are used to filter unreliable liquid water content and N_d retrievals.

2.2 EarthCARE M-NOM and M-COP for spatial context

MSI-based products (M-NOM and M-COP) provide the two-dimensional spatial context required for classifying mesoscale cloud patterns. The M-NOM product contains the calibrated MSI Level 1b reflectances and brightness temperatures (Eisinger et al., 2024). The M-COP product provides cloud optical and physical retrievals, notably cloud optical thickness (COT), effective radius, and cloud-top height (Hünerbein et al., 2024). All products are available at a spatial resolution of 500 m. For the detection of closed and open cells, we use COT from M-COP and the three thermal infrared channel brightness temperatures centred at wavelengths 8.8, 10.8 and 12.0 μm, from M-NOM as inputs for the CNN (described in detail below in Sect. 2.5). Additionally, we compute cloud cover from the M-COP cloud mask (i.e. COT > 0).

https://doi.org/10.5194/egusphere-2026-3000
Preprint. Discussion started: 18 June 2026

2.3 Wind Trajectories to track clouds in time

We compute trajectories, initialized at EarthCARE overpasses over the SEP region in regular distances of 64 km, as this is the distance between CNN scenes (see Sect. 2.6). The trajectories are computed using ERA5 boundary-layer wind fields (Hersbach et al., 2020) and the python package backtrajectory-calculator (Mantilla, 2023), which is based on the Lagrangian method proposed by Stohl (1998). Trajectories are driven by ERA5 winds at 975 hPa (last data access in Jan. 2026), with a temporal resolution of 6 h. We compute wind trajectories 30 hours backward and forward from each EarthCARE overpass to follow the evolution of the observed cloud scene over a 60-hour period.

2.4 GOES for observing the time evolution of cloud structures

Along the trajectories, we use data from the GOES-East Advanced Baseline Imager (ABI) to determine the cloud mesoscale structure, more specifically GOES-16 from Aug. 2024 until 7 Apr. 2025, and GOES-19 since then (Schmit et al., 2017; Group) (data access between 05. Jan. 2026 to 14. Jan. 2026). We use the optical thickness product COD2KMF (ABI-L2), and radiances of the three infrared window channels C11, C14 and C15 centred at wavelengths 8.4, 11.2, 12.3 μm (ABI-L1b), which are converted into brightness temperatures, as inputs for the CNN (described in detail below in Sect. 2.5). All four products have a spatial resolution of 2 km at nadir.

2.5 Classification of cloud mesoscale structure using a CNN

We use fine-tuned versions of the CNN developed by Wu et al. (2025) (last access on 5 Sep. 2025) to classify mesoscale cloud structure. The CNN was originally developed for MODIS and takes as input COT together with three combinations of infrared window brightness temperatures. Each input for the CNN spans 128 km$\times$128 km. In the following, we refer to these 128 km$\times$128 km windows in GOES, MSI, and the corresponding ACM-CAP section along-track, as "cloud scenes". The CNN assigns each scene to one of six mesoscale structure categories following the classification scheme in Yuan et al. (2020): solid stratus, closed mesoscale convective cells (MCC), open MCC, disorganized MCC, clustered cumulus, and suppressed cumulus. In this study, we focus on the closed- and open-MCC categories.

To apply the CNN to MSI and GOES, the input scene data must have a resolution of 1 km, i.e. the original MODIS resolution. To this end, the resolution of the MSI input scenes is reduced from 500 m to 1 km by a 2$\times$2 average-pooling operation, and the GOES input scene data is interpolated from an original resolution of approximately 2 km to 1 km by a weighted mean of nearby original values. The CNN is applied only during daytime. For MSI, this restriction arises because COT is unavailable at night. For GOES, nighttime COT proved incompatible with the network, likely due to fundamental limitations of infrared-only retrievals in capturing high COT values. We only consider scenes without overlying ice clouds. To this end, we check for each scene if there are brightness temperature values below 273 K, and disregard the scene if more than 5% of the pixels within a scene have these low brightness temperatures. Besides the classification into cloud structures, the CNN provides a certainty value between 0 and 1 (see Wu et al. (2025) for details). We filter for cloud scenes that were classified with a certainty value >0.75, which is the case for about 67% of both closed and open cell scenes.

https://doi.org/10.5194/egusphere-2026-3000
Preprint. Discussion started: 18 June 2026

To adapt the network to MSI and GOES, we produce two fine-tuned CNN versions, one for each imager. The fine-tuning is done for the final network layer using manually labeled cloud scenes. Approximately 500 scenes per instrument were labeled according to the six cloud structure classes. Parts of this dataset are withheld from training to evaluate model performance. After fine-tuning, the CNN shows substantially improved classification skill with an F1 score of 0.86 and 0.9 for closed and open cells respectively for the CNN fine-tuned to MSI, and an F1 score of 0.88 and 0.94 for closed and open cells respectively for the CNN fine-tuned to GOES. A detailed evaluation of the fine-tuned CNNs for MSI and GOES is provided in the Appendix A. Examples of the resulting mesoscale cloud-structure classifications for MSI and GOES are shown in Fig. 2 and Fig. 3.

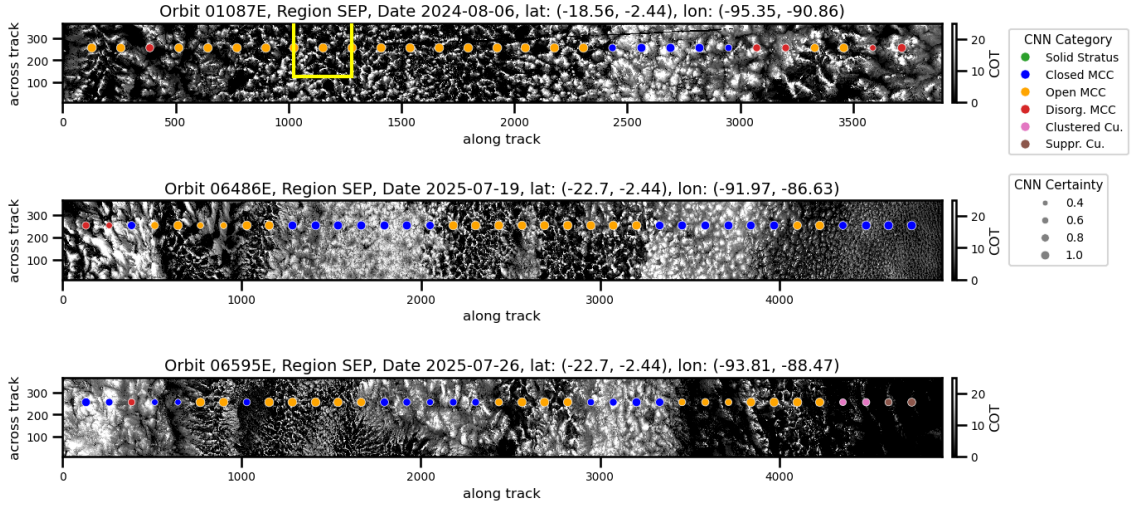

Figure 2. Three example MSI swaths of stratocumulus clouds, with the M-COP COT displayed in grey scale. Coloured dots show the classification into different cloud mesoscale structures by the CNN fine-tuned to MSI; positions of the dots are the midpoints of the classified cloud scenes; sizes of the dots encode the certainty value of the CNN. The yellow square in the upper panel shows the size of the 128 km × 128 km input scenes for the CNN.

2.6 Putting it all together: Dataset of closed and open cell properties with transition information

The CNN fine-tuned to MSI is applied to MSI swaths in all four stratocumulus regions. Scene midpoints are spaced 64 km apart, resulting in overlapping scenes of 128 km (see Fig. 2). This overlap provides a finer structure detection, particularly near cloud structure boundaries. Due to this scene overlap, individual profiles are typically assigned to two neighbouring MSI scenes, and therefore sampled twice. For ACM-CAP, we compute the mean and coefficient of variation (CV = standard deviation / mean) for different cloud and precipitation properties for each of these along-track 128 km scenes. For the computation of mean and CV for cloud properties (CTH, CBH, LWP, N_d and r_e), we consider only cloudy profiles. Likewise for the computation of mean and CV of rain properties (RWP and D_0) we consider only raining profiles. Additionally, we define a binary rain occurrence for each scene, counting a scene as rainy if any of its profiles show rain. We also compute a rain fraction, i.e. the relative frequency of rainy profiles within a scene.

https://doi.org/10.5194/egusphere-2026-3000
Preprint. Discussion started: 18 June 2026

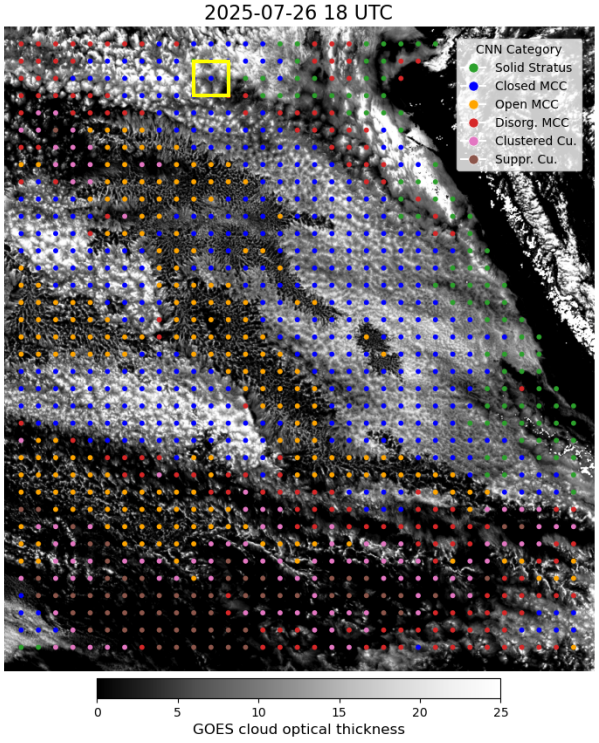

Figure 3. Example GOES/ABI image of the SEP stratocumulus region, with GOES COT displayed in grey scale. Coloured dots show the classification into different cloud mesoscale structures by the CNN fine-tuned to GOES; positions of the dots are the midpoints of the classified cloud scenes. The yellow square in the upper part of the image shows the size of the 128 km × 128 km input scenes for the CNN.

The resulting dataset contains scenes classified into one of the six mesoscale structure classes, including open and closed cells, and cloud property information from ACM-CAP per scene for all four stratocumulus regions. Overall, the dataset contains about 5000 scenes of closed cells, and about 2500 scenes of open cells. Fig. 1 shows the geographic distribution of closed and open cells in the four stratocumulus regions, computed from this dataset. Closed cells occur most frequently in near-coastal regions, whereas open cells typically occur more offshore, consistent with previous findings (Muhlbauer et al., 2014; Mohrmann et al., 2021; Wu et al., 2025).

For the SEP region, we retrieve additional information about the temporal development of cloud structures around the EarthCARE overpasses. To this end, we apply the CNN to GOES imagery along the computed wind trajectories. More specifically, we interpolate the trajectories to a temporal resolution of two hours and use the corresponding GOES data for 128 km×128 km scenes around the position of each trajectory. We then apply the fine-tuned CNN to these scenes to determine the cloud structure. Figure 4 illustrates this approach for a single EarthCARE overpass. An animation of this example, showing all time steps, is provided in the supplementary material.

https://doi.org/10.5194/egusphere-2026-3000
Preprint. Discussion started: 18 June 2026

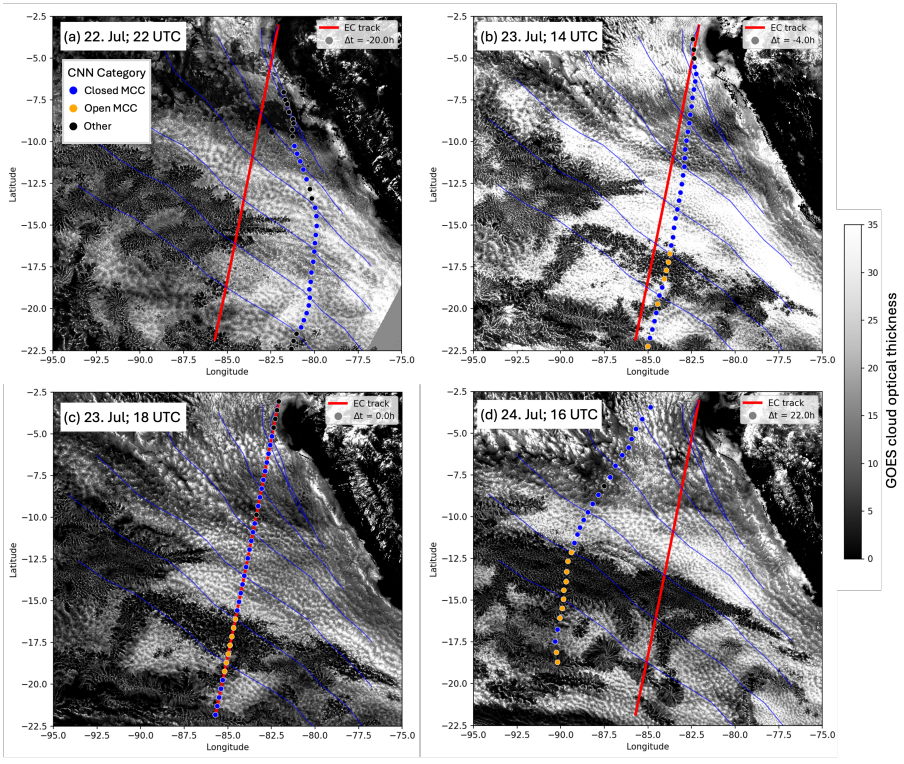

Figure 4. Example illustrating the method used to track cloud structure evolution along trajectories. The panels show GOES COT for four time steps between 22 July to 24 July 2025. The red line shows the location of the EarthCARE overpass, which happened around 18 UTC on 23 July. Trajectories are initiated at the time of the EarthCARE overpass (c) and tracked backwards (a,b) and forwards (d) in time. The coloured dots represent the midpoints of each tracked cloud scene (128 km×128 km), with colours indicating the mesoscale cloud type retrieved by applying the CNN to the GOES imagery. Thin blue lines indicate the full trajectories for a subset of these scenes.

For each tracked cloud scene, we identify whether a transition from closed to open cells occurs and record the timing of this transition. In the example in Fig. 4, a pocket of open cells has formed by the time of the EarthCARE overpass at latitudes $-15°$ to $-20°$ (Fig. 4(c)). Using the trajectories, we trace the observed open cells back to the moment when they formed. Figures 4 (a, b) show, for example, that the pocket of open cells had not yet formed 20 h before the EarthCARE overpass and was smaller in size 4 h before the overpass. Conversely, some scenes are classified as closed cells at the time of the EarthCARE overpass, and transition to open cells later (in Fig. 4(d) due to the increasing size of the pocket of open cells). Again, we identify whether a transition occurs in these cloud scenes and determine its timing. As described in Sect. 2.5, the CNN classification for GOES is only available during daytime. For transitions occurring during nighttime – i.e. when a scene is classified as closed cells at the last available time of day 1 and as open cells at the first available time of day 2 – we pinpoint the time of transition using the brightness temperature of the 11.2μm GOES channel: As cloud fraction is expected to decrease rapidly during a transition

https://doi.org/10.5194/egusphere-2026-3000
Preprint. Discussion started: 18 June 2026

from closed to open cells, we define the time during the night when the change in brightness temperature is maximal as the transition time.

Overall, we find 803 trajectories for which transitions from closed to open cells occur; 330 of which are closed cells at the time of the EarthCARE overpass and transition to open cells at a later point in time, and 473 are open cells at the EarthCARE overpass and could be traced back to their previous closed-cell state. Figure 5 shows all of these trajectories. It shows that trajectories go, as expected in the SEP region, typically from South-East to North-West. Transitions were found throughout the studied region, with the majority being located relatively central to it. Figure 6 shows that transitions were mainly found during the time period from June to October, consistent with previous satellite observations that show that the frequency of occurrence of both closed and open cells is highest during these months (Muhlbauer et al., 2014).

Note that it is not feasible to estimate the time evolution of cloud scenes by collecting several EarthCARE overpasses along a trajectory (as was done e.g. by Eastman et al. (2022) for MODIS data), since the active instrument swath is narrow and very rarely coincides with the position of a trajectory more than once. Therefore, the approach of combining EarthCARE with GOES was chosen, which has the additional advantage that, due to the high temporal resolution of GOES, it is possible to pinpoint the timing of the transition to a narrow time range.

3 Results

3.1 Properties of closed and open cells

In this section, we analyse the similarities and differences between closed and open cells in terms of their cloud properties, as determined by ACM-CAP. To illustrate the cloud and rain products, and the variability withing cloud scenes, Fig. 7 shows example scenes of typical closed and open cells from ACM-CAP and M-COP. As described in Sect. 2.6, we compute the mean and CV of cloud and rain properties for each 128 km along-track cloud scene in ACM-CAP (see Fig. 7). The statistics of scene-mean and CV for all scenes from all stratocumulus regions are shown in in Fig. 8. In Appendix B, we additionally present statistics of the median, and 5th, 25th, 75th and 95th percentiles of all closed and open cell scenes, since mean and CV alone cannot capture all aspects of a distribution.

We start with analysing the vertical structure of clouds. Figure 7 shows that the vertical extent in terms of average cloud base height (CBH) and cloud top height (CTH) is similar for the closed and open cell examples. It also shows that the CTH and CBH of the closed cells remain stable across the scene, whereas the open cells exhibit greater variability, with thin cloud layers existing between thicker cells. These thin cloud layers are usually found at the minimum CBH or maximum CTH level. This indicates that they may be new cells forming or remnants of old cells, respectively. The vertical structure features in the example scenes are typical of the overall statistics over all data in the four stratocumulus regions (see Fig. 8). The distributions of mean CTH and CBH show only small differences. Open cell CTHs are slightly higher (about 200 m on average), and this relatively small difference reduces even to 60 m, when stratifying by longitude and season for each stratocumulus region (not shown). The mean CBH difference between open and closed cells, when stratified by longitude and season, is only 10 m (not shown). The higher CV of both CBH and CTH reflects the highly variable vertical structure of open cells, which consists of

https://doi.org/10.5194/egusphere-2026-3000
Preprint. Discussion started: 18 June 2026

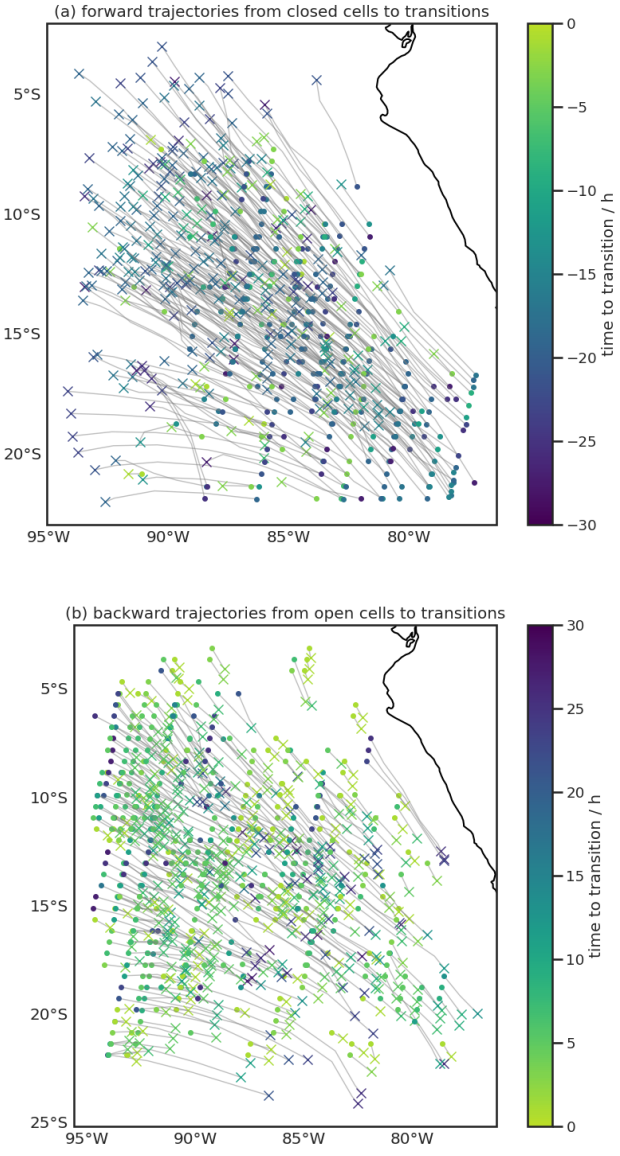

Figure 5. All trajectories for which closed-to-open cell transitions were found. (a) Trajectories for cloud scenes that were closed cells at the time of the EarthCARE overpass and later transitioned to open cells; (b) trajectories for open-cell scenes at time of the EarthCARE overpass that could be traced back to a transition from closed cells at an earlier time. Dots mark positions of scenes at EarthCARE overpasses; crosses mark positions of transitions. The color encodes the time difference between overpass and transition.

https://doi.org/10.5194/egusphere-2026-3000
Preprint. Discussion started: 18 June 2026

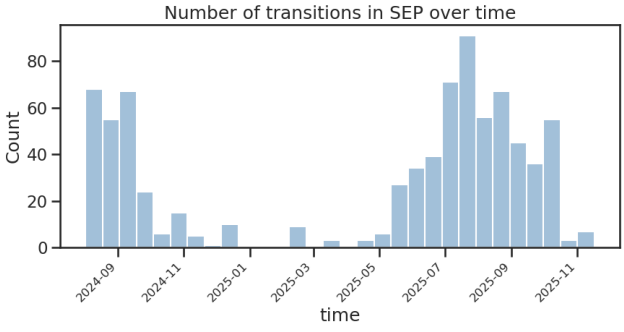

Figure 6. Number of closed-to-open cell transitions identified in the combined EarthCARE-GOES dataset as a function of time.

thin layers interspersed with thicker cells. These findings on vertical structure broadly agree with previous findings. Wood et al. (2011), who analysed a POC and surrounding closed cells from aircraft measurements found high variability in CBHs of open cells, (even though they find less variable CTHs). Smalley et al. (2022) found that the planetary boundary layer height is similar for POC and surrounding closed cells. McCoy et al. (2017) provides an indirect indication of the presence of thin cloud layers between thicker open-cell clouds, finding that open cells have a lower albedo than closed cells for the same cloud fraction.

Next, we analyse the cloud microphysical properties. The examples in Fig. 7 illustrate that the LWP is spatially more homogeneous for closed cells. In open cells it is much more variable, with LWP values significantly higher in some regions than in others. In the overall statistics, the mean LWP per scene is similar for both closed and open cells, but open cells have a higher CV, i.e. they have more “extreme" values of LWP, both smaller and larger. A similar pattern can be seen with r_e: closed cells exhibit highly homogeneous r_e, whereas open cells demonstrate greater variability. While the mean r_e is similar for both types of cell, as with LWP, open cells exhibit greater variability and “extreme" r_e values. N_d on the other hand shows a large difference between closed and open cells in mean values, with open cells having very low N_d values of 10 to maximally 100 cm^{-3}. The findings of similar LWP and lower N_d for open cells fit to previous satellite studies using passive imagers (Wood et al., 2008; Smalley et al., 2022). However, previous studies have often found larger average r_e in open cells, (e.g. Stevens et al. (2005); Rosenfeld et al. (2006); Wood et al. (2008); Watson-Parris et al. (2021); Smalley et al. (2022)), whereas we find that the average r_e value does not change but the variability of r_e gets larger with more large particles, but also more small particle sizes. It is possible that the passive imagers, as used in previous studies, are unable to detect the very small particles, that we see in ACM-CAP, since they are usually found in the optically thin parts of the open cells and are often below the typical detection limit of about 5 μm for Nakajima-King-like retrievals for passive imagers (Nakajima and King, 1990).

A plausible physical explanation for the microphysical differences between closed and open cells comes from LES simulations (e.g. Wang and Feingold, 2009a; Chandrakar et al., 2022): In closed cells, there are typically many CCN available (as confirmed by aircraft measurements (Petters et al., 2006; Wood et al., 2011; Terai et al., 2014)). Updrafts and high supersaturation lead to the activation of many droplets, which compete for water vapor. These droplets stay small in size and with a

https://doi.org/10.5194/egusphere-2026-3000
Preprint. Discussion started: 18 June 2026

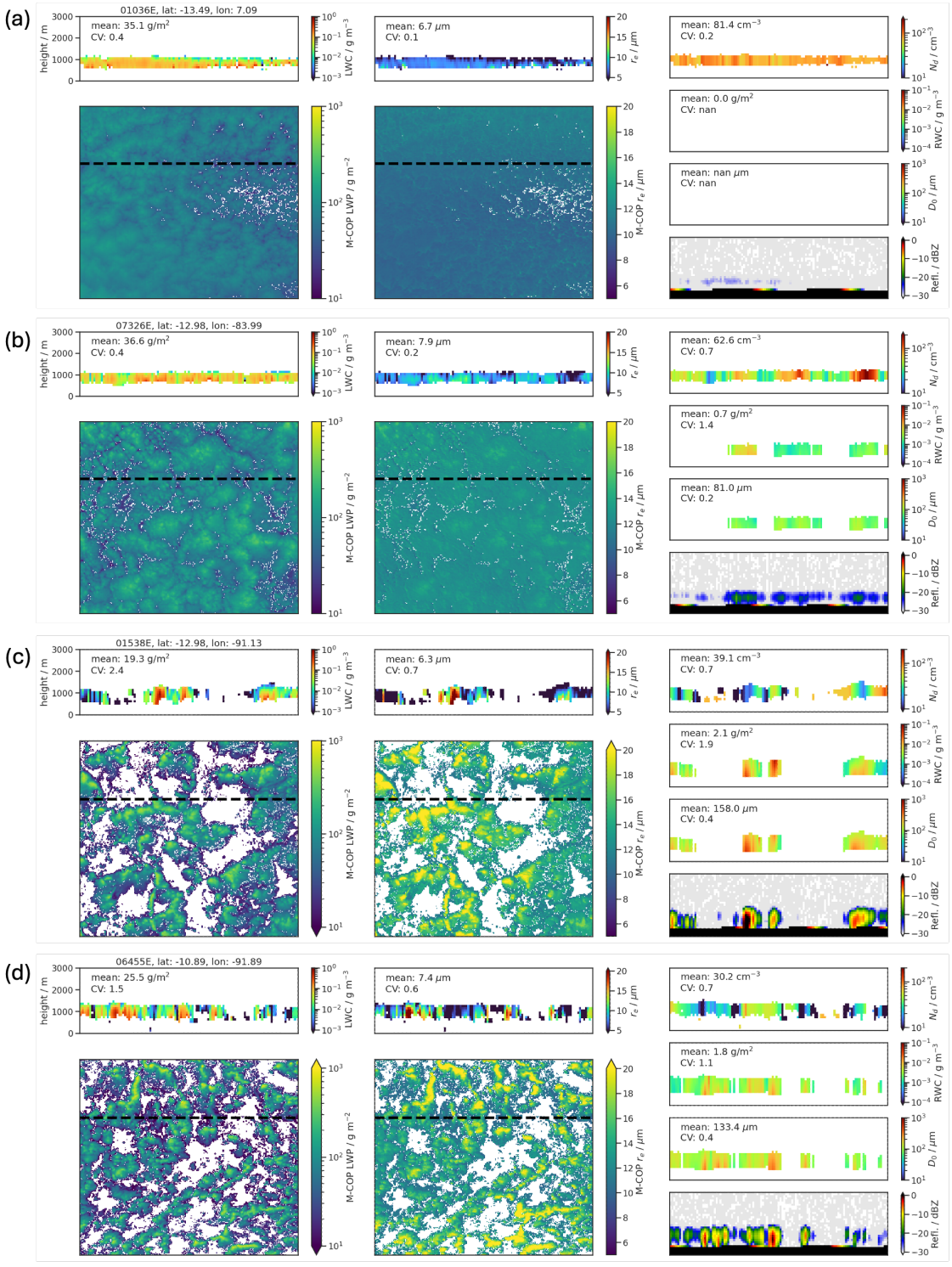

Figure 7. Examples of typical closed (a,b) and open (c,d) cells cloud scenes of 128 km×128 km in M-COP, and the corresponding ACM-CAP section along-track (black dashed line in M-COP images) for several cloud and rain variables. The orbits and mid-points of the scenes are specified in the titles. Numbers at the top left in ACM-CAP scenes are the mean and CV taken over the 128 km along-track scenes. The bottom right panel in each subfigure shows the CPR reflectivity.

https://doi.org/10.5194/egusphere-2026-3000
Preprint. Discussion started: 18 June 2026

narrow droplet size distribution. In open cells, there are fewer CCN available due to rain scavenging. This leads to fewer cloud droplets, as well as to broader size distributions.

An interesting feature, that we see in many M-COP examples of non-precipitating closed cells, is the horizontal distribution of r_e within individual cloud cells: r_e is largest at the edges of the cells and smallest at the centre, where the updraft is located - even though the difference is small, it is consistent through many examples we analysed (see M-COP r_e in Fig. 7(a) as an example). An explanation might be that droplets are older in downdrafts than updrafts (de Lozar and Muessle, 2016; Chandrakar et al., 2022, who showed larger droplet ages in downdrafts for open cells) and might therefore have more time to grow to (slightly) larger sizes. For precipitating closed cells and open cells, the horizontal r_e distribution is reversed, with larger r_e at the positions of updrafts (see M-COP r_e in Fig. 7(b-d)).

Lastly, we analyse the rain properties. Open cells show a higher frequency of rain occurrence and higher RWP compared to closed cells, which fits well with smaller N_d, higher variability of droplet sizes and greater extremes in LWP. However, note that closed cells also drizzle in about 60% of scenes, albeit often only lightly. More heavy rain (RWP $> 20\,\mathrm{gm}^{-2}$) is rarely found in closed cells, but often occurs in open cells (see 95th percentile distribution in Appendix B). The rain fraction shows a broad distribution for both closed and open cells. Especially for open cells, the sampling nature of active instruments may be partly responsible for this broad distribution, since in some cases the satellite passes directly over the centres of raining cells; in other cases it may sample mainly cloud edges or optically thinner areas. For closed cells, the most common cases are only few raining profiles, i.e. rain fraction close to zero, and rain fractions close to one. Lastly, rain drops are larger in open cells. The size of raindrops has implications for virga depth and surface rain rates, since larger droplets are more likely to reach the surface. This, in turn, implies stronger aerosol scavenging. The higher CV of rain drop sizes is due to a higher number of large raindrops in open cells; small raindrop sizes are equally frequent in closed and open cells (see 25th and 75th percentile distribution in Appendix B).

Higher rain rates in open cells compared to closed cells have also been found in previous studies using CloudSat and AMSR/E (Muhlbauer et al., 2014; Eastman et al., 2022), as well as ground based measurements (Jensen et al., 2021) and aircraft campaigns (Wood et al., 2011; Terai et al., 2014). The bigger surprise is the high rain occurrence in closed cells, which have in the past often been considered as non-raining. This notion may stem from the fact that most field studies have sampled clouds relatively close to the coast with small CTHs and consequently lower probability of rain, as shown by Possner et al. (2020). EarthCARE's high sensitivity enables the rain properties of low-level clouds to be quantified and studied in great detail for the first time from a satellite. As mentioned in Sect. 2.1, EarthCAREs drizzle detection is highly improved and able to detect even light drizzle, that might have gone undetected before. Our finding that (light) drizzle is prevalent in closed cells, is to a large extent thanks to this improved sensitivity (Xu et al., 2025). It should be noted here that, as the other variables, the frequency of rain is computed on a scene basis, i.e. a scene is counted as raining if at least one profile within the 128 km scene shows rain. This may lead to higher values for rain occurrence in closed cells with sparse precipitation than if we were to count rain profiles in the original 1 km resolution. However, Fig. 8 shows that high rain fractions are also relatively common in closed cells, and we believe that scene-based rain occurrence is a more relevant measure for capturing mesoscale cloud properties.

https://doi.org/10.5194/egusphere-2026-3000
Preprint. Discussion started: 18 June 2026

The measurement of rain drop sizes, D_0, are also strongly improved for EarthCARE: The Doppler measurements are strongly dependent on particle sizes, and therefore help to determine both rain rates and drop sizes (Mason et al., 2017, 2023).

As described above, closed and open cells exhibit similar mean LWP, yet open cells show substantially larger RWP. This indicates that the LWP-RWP relationship differs between the two cloud regimes, as examined in Fig. 9. For a given LWP, open cells consistently produce higher RWP than closed cells, implying a markedly greater efficiency in rain formation. This behavior is robust across all four stratocumulus regions analysed. The enhanced RWP in open cells is primarily driven by larger raindrop sizes rather than by increased raindrop number concentrations. These statistics align with observations of individual cases: we find open-cell examples exhibiting intense precipitation even at low LWP, including instances where RWP exceeds LWP (e.g., the left-most and central cells in Fig. 7 (c)). Such cases likely represent decaying cells in which a substantial fraction of cloud water has already been converted into rain. Similar phenomena have been reported in airborne observations by Wood et al. (2011).

Summarizing, EarthCARE provides detailed observations on vertical structure and microphysics of cloud and rain for closed and open cells. The two cloud structures show large differences in their microphysics, most notably lower N_d and stronger rain in open cells.

3.2 Transitions from closed to open cells

A polar-orbiting satellite such as EarthCARE provides only instantaneous measurements of cloud properties at the time of overpass. As described in Sect. 2.6, we combine these instantaneous observations with backward and forward trajectories, as well as GOES/ABI geostationary imagery, to reconstruct the temporal evolution of individual cloud scenes. This analysis focuses on the SEP region, where most transitions between open and closed cells occur.

To illustrate clouds and their properties around the transition time with an example, Fig. 10 shows M-COP and ACM-CAP variables for four neighboring cloud scenes. Clouds in the left two scenes have (mostly) transitioned to open cells shortly before (1 h) the overpass, and the clouds in the right two scenes transition to open cells shortly after (1 h and 3 h respectively) the overpass, as determined by tracking them in GOES. Note the large r_e, low N_d and high RWC in the closed cells, compared to typical non-transitioning closed cells as shown in Fig. 7. More example scenes, ordered by their time to transition, can be found in the Appendix C.

Figures 11 and 12 present all cloud scenes in which closed-to-open cell transitions were identified. The figures show cloud and rain properties retrieved from EarthCARE, plotted as a function of their time to transition. Figure 11 (a) shows the number of cloud scenes that were found for different time-to-transition values. The EarthCARE overpass, and therefore the time of measurement, is always around 13:00 local time in the SEP region. Different time-to-transition values therefore mean that the transition happened at different times of the day. A first observation to note in Fig. 11 (a) is that transitions were found at almost all time-to-transition values, hence transitions can happen at any time of the day. A transition occurring between 5 to 19 hours before or after the overpass, means local nighttime. Adding all transition counts during daytime and nighttime in Fig. 11 (a) shows that the majority of transitions occur during nighttime (around 60 %), consistent with Wood et al. (2008). Furthermore, the number of transitions show an interesting pattern with peaks at dawn (e.g. a time to transition of -19 means that a transition

https://doi.org/10.5194/egusphere-2026-3000
Preprint. Discussion started: 18 June 2026

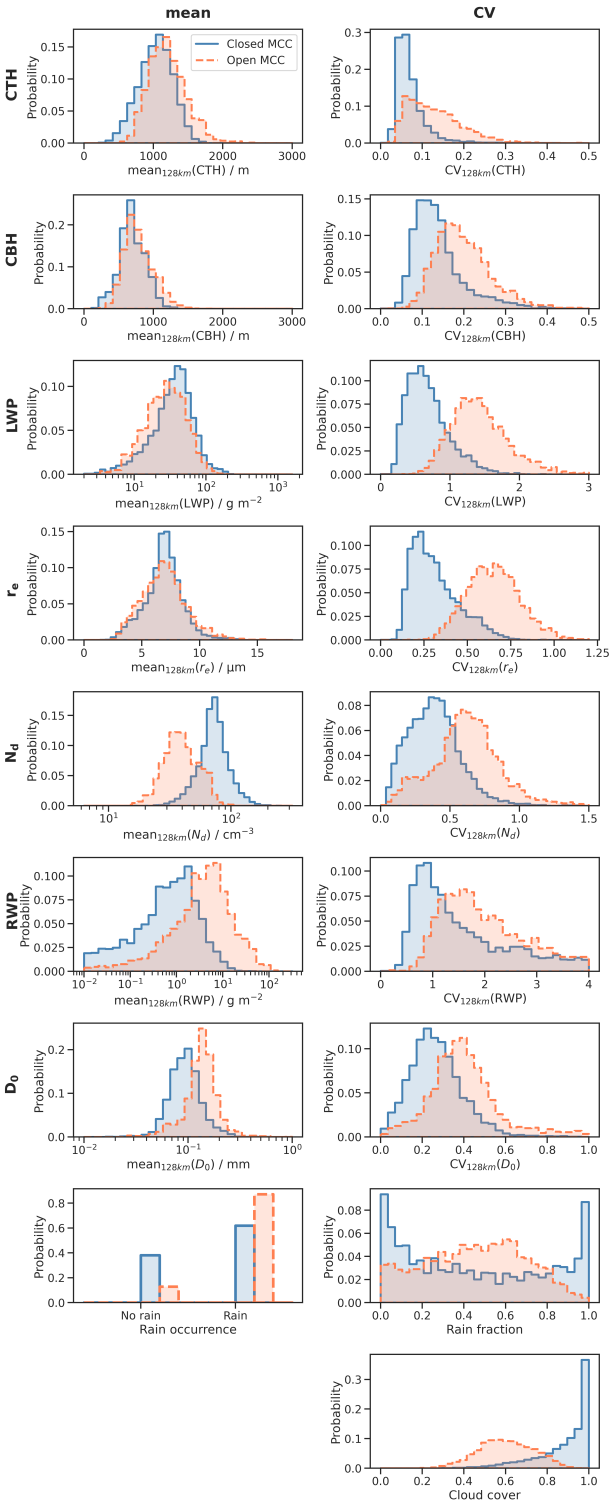

Figure 8. Probability distributions of cloud and rain properties of closed and open cells over all stratocumulus regions. For the upper seven rows, panels in the left column show the distribution of mean values over 128 km scenes; panels in the right column show the distribution of CVs. The lowermost two rows show rain occurrence, rain fraction for raining scenes, and cloud cover.

https://doi.org/10.5194/egusphere-2026-3000
Preprint. Discussion started: 18 June 2026

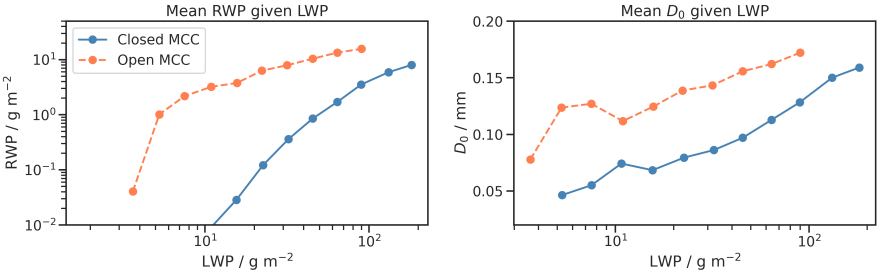

Figure 9. Mean RWP and D_0 per LWP bin for closed and open cells. The mean is computed over all four stratocumulus regions.

to open cells happened 19 h after the EarthCARE overpass, hence around 08:00 local time. A time to transition of 5 means that the transition to open cells happened 5 h before the EarthCARE overpass, i.e. again around 08:00 local time).

Fig. 11 (b) shows cloud cover, derived from M-COP. As expected, cloud cover is near unity for closed cells and drops to much lower values, around 0.6, after clouds transition to open cells. Both CTH and CBH remain relatively constant and do not show notable deviations from their climatological values around the transition time. Their CV remain stable until the transition and increase only at the transition to values typical for open cells (dashed line in Fig. 11 (b)).

In contrast, LWP, r_e and N_d show a distinct temporal evolution already long before the transition (see Fig. 12 (a-f)). LWP begins to increase approximately 25 h before the transition, peaks near the transition time, and subsequently decreases as open cells form – consistent with the emergence of thinner cloud layers characteristic of open-cell structure. In parallel to LWP, r_e increases with a peak shortly before the transition and decreases thereafter. As for LWP, the decrease is consistent with the emergence of thin cloud layers with small droplet sizes between the thicker open cell clouds. N_d steadily decreases toward the low climatological values of open cells. For both r_e and N_d, the deviations from their climatological closed-cell values seem to begin slightly later than for LWP, around 20 h before the transition. However, since the number of observed cases at these time-to-transition values are few (see Fig. 11a), it is difficult to draw a definite conclusion about the exact timing. The CV for LWP, r_e and N_d is relatively stable around the climatological values for closed cells and increases only shortly before the time of the transition. Hence, although the mean values of cloud microphysical parameters begin to change well before a transition occurs, they remain relatively homogeneous, i.e. at CV values typical of closed cells. It is only around the time of the transition that they begin to show stronger variations.

Smalley et al. (2022), who track transitions using GOES imagery, similarly report decreasing N_d and increasing r_e before transitions. However, they find relatively constant LWP and a continued increase in r_e after open cells have formed. As noted earlier, these differences may arise from limitations in passive retrievals, especially regarding thin cloud layers and small droplets, which tend to bias retrieved LWP and r_e toward higher values in open-cell conditions.

As with cloud microphysics, changes in rain properties occur well before the transition. RWP is already slightly elevated approximately 25 h before transition and increases to near open-cell climatological values approximately 10 h before the transition. In contrast to r_e and N_d, which show the strongest rates of change shortly before the transition, the increase in RWP

https://doi.org/10.5194/egusphere-2026-3000
Preprint. Discussion started: 18 June 2026

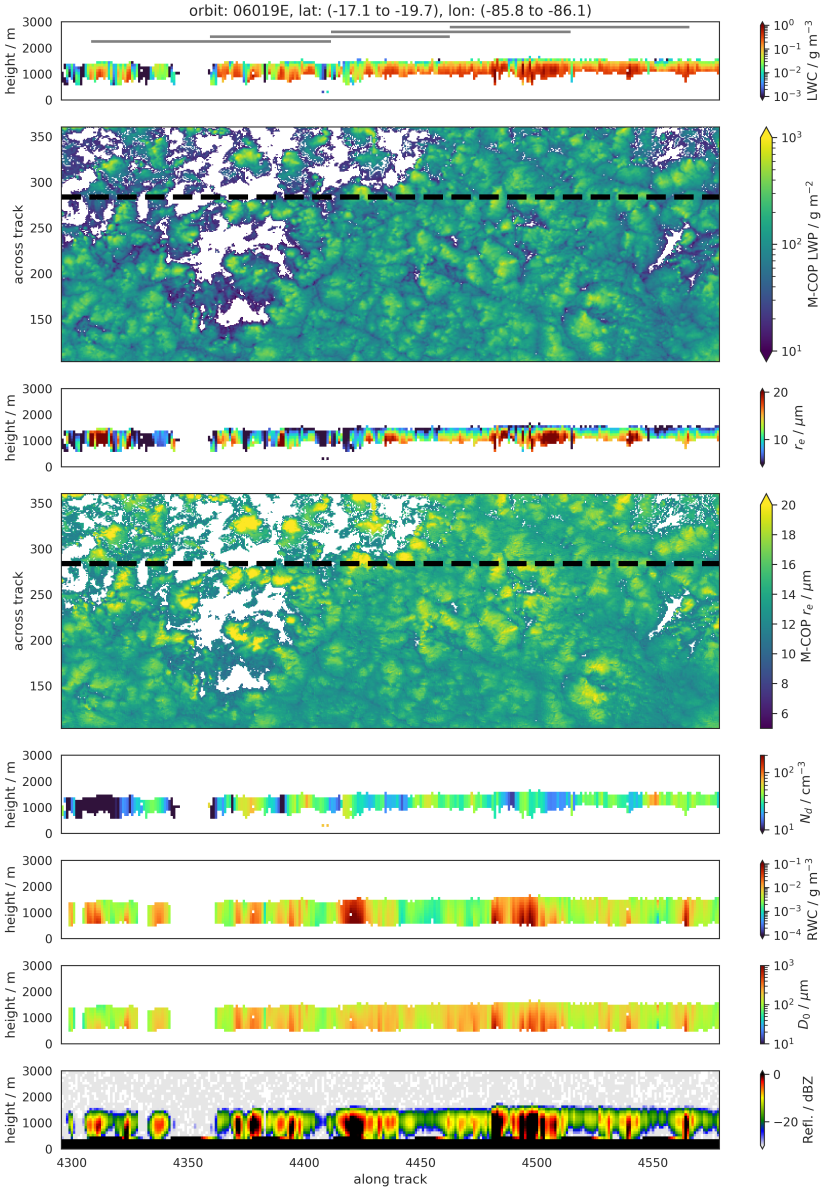

Figure 10. Example illustrating cloud and rain properties from M-COP and the corresponding ACM-CAP section along-track (black dashed line in M-COP images), together with CPR reflectivity, for clouds shortly before and after transition to open cells. The figure consists of four neighbouring cloud scenes, whose extent along track is shown by the grey lines in the uppermost panel. For the leftmost two scenes, much of the cloud field had transitioned to open cells shortly (1 h) before the overpass, whereas on the right, transition occurred shortly afterward (1 and 3 h for the two scenes respectively).

https://doi.org/10.5194/egusphere-2026-3000
Preprint. Discussion started: 18 June 2026

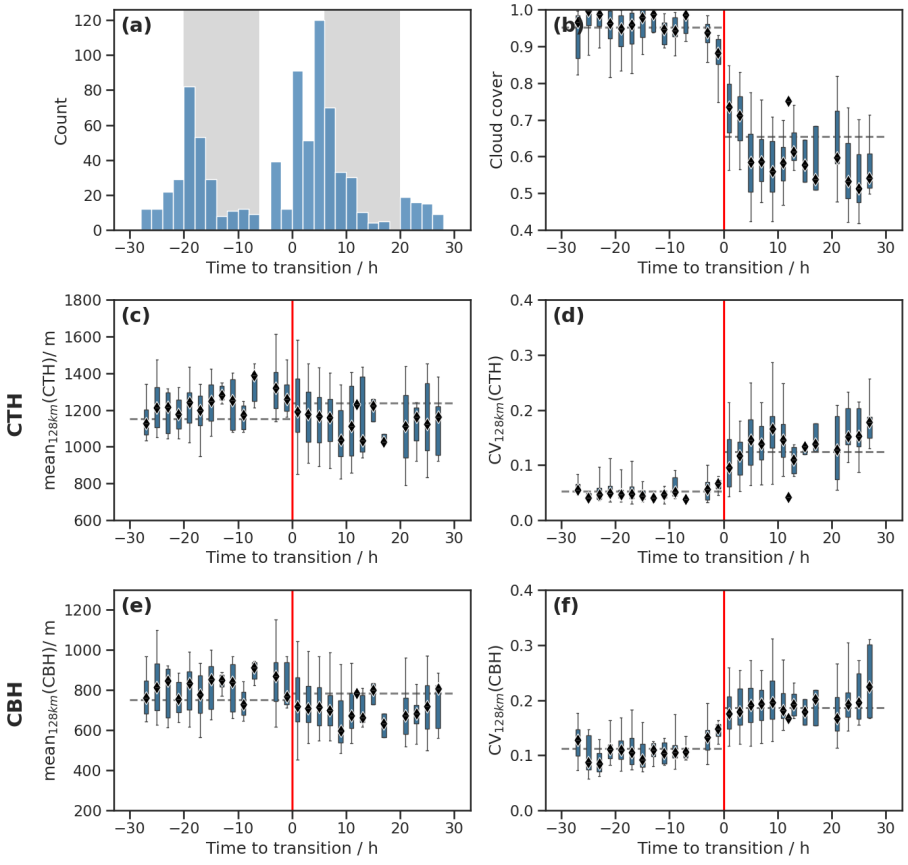

Figure 11. Cloud properties of all cloud scenes in which closed-to-open cell transitions were identified, as a function of their time to transition (= time of EarthCARE overpass − time of transition). Negative time-to-transition values correspond to clouds that were still closed cells during the EarthCARE overpass and transitioned subsequently, while positive values correspond to scenes that had already transitioned prior to the overpass and could be traced back to an earlier transition time. (a) number of cloud scenes that were found for different time-to-transition values. Grey shading indicates local nighttime. (b) cloud cover computed from M-COP; (c-f) cloud vertical structure from ACM-CAP. The box plots in (b-f) represent the distribution of $\text{mean}_{128\text{km}}$ and $\text{CV}_{128\text{km}}$ values of cloud parameters for all scenes with the same time-to-transition. Black diamonds indicate the medians of these distributions. The blue bars indicate the values between 25th and 75th percentile, whiskers are from 5th to 95th percentile. Horizontal dashed, grey lines indicate the "climatological" median values for closed and open cells, derived from the closed and open cell distributions in Fig. 8. These serve as a reference for comparing with the medians of the box plots (i.e. of the cloud scenes for which transitions were identified).

https://doi.org/10.5194/egusphere-2026-3000
Preprint. Discussion started: 18 June 2026

slows down from around 10 h before the transition. D_0 steadily increases toward the higher climatological values of open cells. This increase of D_0 seems to begin a few hours later than for RWP, around 20 h prior to the transition, following a similar timeline as changes in r_e and N_d. However, as mentioned above, the precise timing should be viewed with a degree of caution and is more speculative than the overall quite clear trend.

Because increases in average RWP may have multiple origins, we analyse additional rain-related quantities in Fig. 13. All rain-related quantities, rain fraction (i.e. relative frequency of raining profiles compared to cloudy profiles), RWP below cloud base and RWC at cloud base, show increased values before transition. This means that the increase in RWP is both due to higher rain intensities and more clouds producing rain. While rain fraction and RWP below cloud base plateau in the hours leading up to the transition (around 10 h before transition), the RWC at cloud base is still increasing, particularly the 95th percentile values. Hence, shortly before transitions, the increase in rain is mainly due to an increase in the "extremes", with stronger, more clustered rain events (see also CV(RWP) in Fig. 12).

4 Discussion

4.1 Interpretation of the transition timeline

From the sequence of deviations from climatological values, we propose a timeline of physical processes leading to closed-to-open cell transitions (see Fig. 14). We hypothesise that the early increase in LWP and, as a consequence, RWP is due to increased moisture in the boundary layer – consistent with Eastman et al. (2022), who found that transitions are preceded (for lead times of $\tilde{3}$ days) by strong surface winds that increase boundary layer moisture. After rain intensifies and begins to reach the surface, aerosols in the boundary layer are scavenged, reducing N_d and increasing r_e as a consequence. This promotes further precipitation, sustaining a rain-aerosol-scavenging feedback. After several hours of intensified rain, the rainfall becomes more clustered, with higher peak rain rates and large D_0, until the cold, moist air generated by evaporation becomes strong enough to reorganise the mesoscale cloud structure into open cells. Hence, we hypothesize that increased moisture is a possible initial trigger for the transition, leading to intensified rain which is further amplified by the aerosol scavenging–rain feedback. Note that the the whole transition process following this timeline takes a long time; around 25 h.

Alternative hypotheses in the literature propose that transitions are initiated by low aerosol availability. In LES studies in particular, aerosol number concentration is often used as a control parameter to nudge the stratocumulus system to the closed or open cell state. However, our results suggest that low aerosol availability is not a prerequisite for transitions. Initially, the transitioning clouds still exhibit climatological values of N_d, and the subsequent decrease in N_d occurs in tandem with other microphysical parameters, possibly due to the proposed aerosol scavenging–rain feedback.

The diurnal cycle of the number of transitions (see Fig. 11a)) provides additional insight into the underlying processes. The observed peak in transitions around dawn may be linked to the diurnal evolution of LWP. In closed-cell stratocumulus, radiative cooling at cloud top is the primary driver of boundary-layer circulation. During nighttime, the absence of solar radiation enhances this cooling, leading to a gradual increase in LWP with a maximum near dawn. Given the close relationship

https://doi.org/10.5194/egusphere-2026-3000
Preprint. Discussion started: 18 June 2026

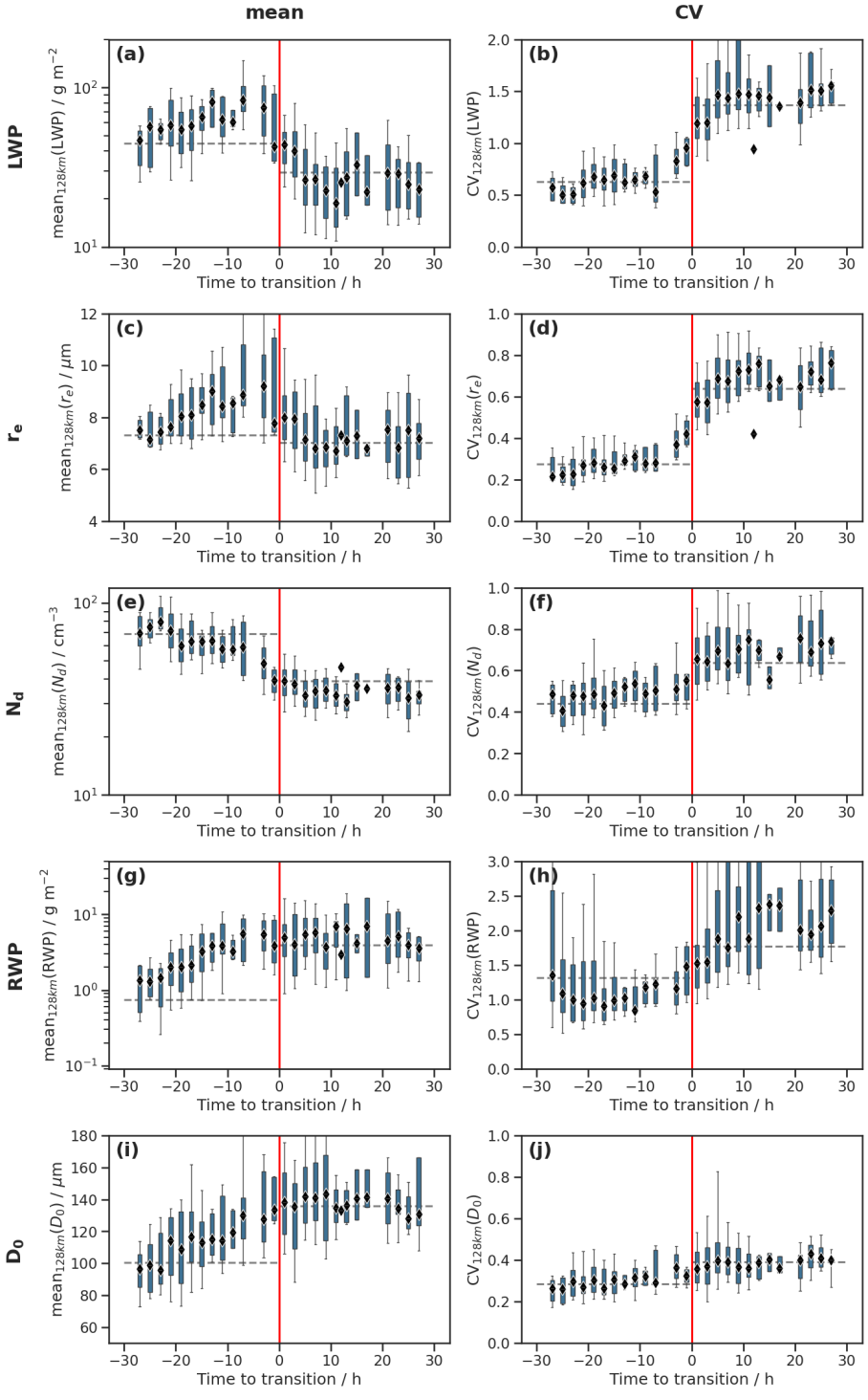

Figure 12. Same as Fig.11 (b-f), but for cloud microphysical and rain properties from ACM-CAP.

https://doi.org/10.5194/egusphere-2026-3000
Preprint. Discussion started: 18 June 2026

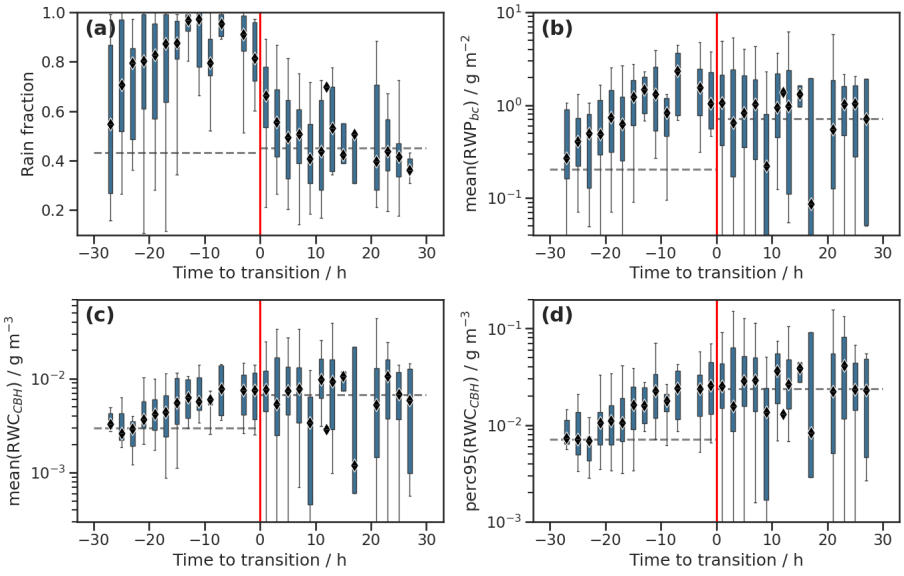

Figure 13. Same as Fig.11 (b-f), but for (a) rain fraction, (b) mean RWP below cloud, (c) mean rain water content at cloud base and (d) 95th percentile of rain water content at cloud base, from ACM-CAP.

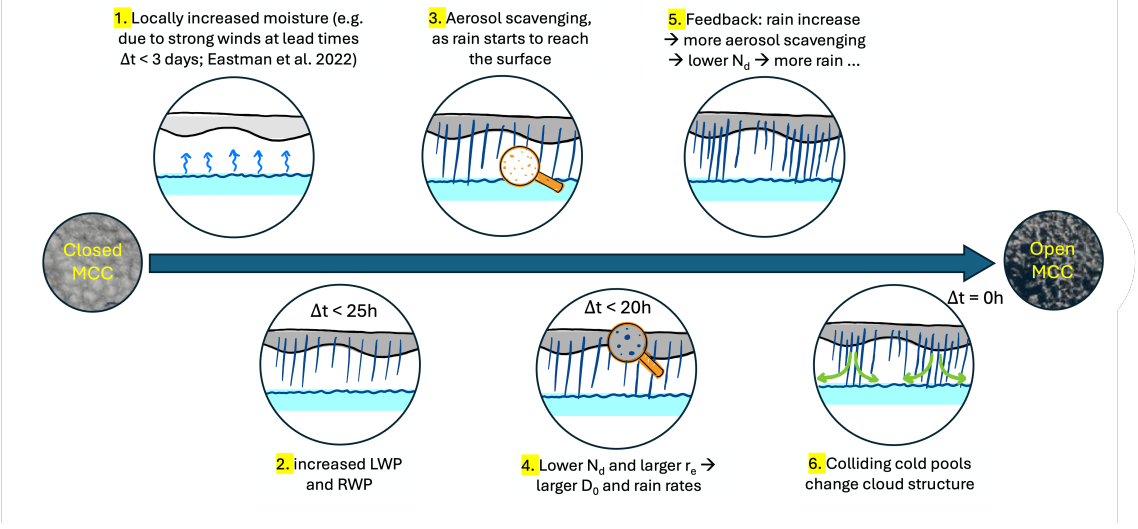

Figure 14. Hypothesised timeline for the processes leading to a transition from closed to open cells.

https://doi.org/10.5194/egusphere-2026-3000
Preprint. Discussion started: 18 June 2026

between LWP and RWP, precipitation is also expected to peak at this time. This behaviour is consistent with our interpretation of a precipitation-linked transition pathway.

An open question is whether the onset of incoming radiation at sunrise also actively contributes to the transition. One possible mechanism is that shortwave radiation weakens the radiatively driven circulation of closed cells, thereby facilitating a shift toward open-cell dynamics. Assessing the relative roles of nocturnal cooling and daytime radiative effects in triggering transitions will require further dedicated investigation.

Finally, we discuss the occurrence of cold pools in a case study. To this end, we employ measurements of the Sentinel-1 satellite. Sentinel-1 carries a C-band Synthetic Aperture Radar (SAR) that provides high-resolution measurements of the surface independent of cloud cover. Over the ocean, SAR can reveal cold pools because the strong surface winds at the edges of cold pools roughen the sea surface, producing characteristic ring- or arc-shaped patterns in the polarized radar backscatter. The Sentinel-1 acquisition pattern primarily measures land and coastal waters; acquisitions over the open ocean are mostly limited to storm occurrences. This unfortunately makes measurements at open cell positions rare, as they usually occur further downwind to the west (see Fig. 1). We however found one example, shown in Fig. 15. Cold pools on the ocean surface are clearly visible in the SAR image and are in the same position as open cells in the corresponding GOES image. While these images demonstrate the presence of cold pools in open cell regimes, they cannot prove that cold pools are responsible for the formation or maintenance of open cell structures. Nevertheless, they provide additional observational evidence. A future study could examine wind speeds from SAR as a function of time-to-transition, using geostationary satellites in a similar synergistic way to this study. It would be interesting to determine at what stage in the time development cold pools emerge.

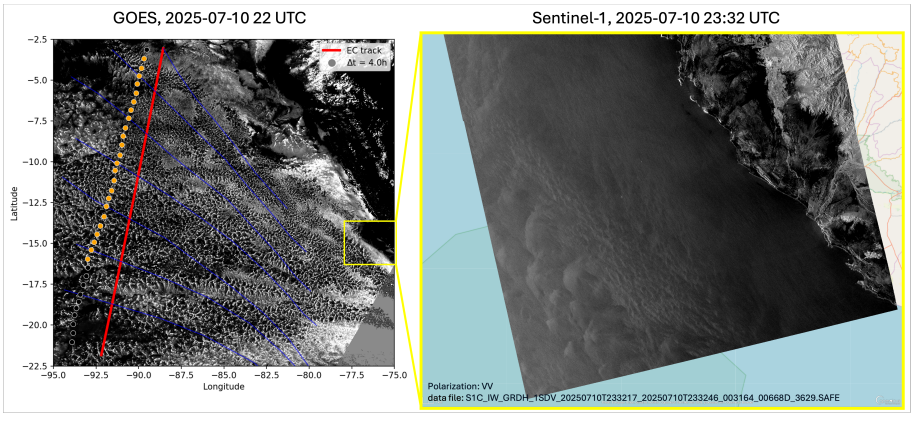

Figure 15. Example for cold pools measured from the Sentinel-1/SAR instrument, accessed from the Copernicus browser (https://browser.dataspace.copernicus.eu/, last access on 13.03.2026); variable shown is "VV decibel gamma 0". The GOES image gives spatial context, showing the whole SEP region, with the position of the SAR image shown as yellow rectangle. It shows that cold pools are at the position of the open cells. As in Fig. 4, the position of the EarthCARE overpass is shown as red line, and the position of the cloud scenes tracked to 22 UTC is shown in the coloured dots.

https://doi.org/10.5194/egusphere-2026-3000
Preprint. Discussion started: 18 June 2026

4.2 Implications

Our results, supported by previous work by Eastman et al. (2022), suggest that increased moisture in the boundary layer is a potential trigger for increased rain leading to a transition. This implies that changes in environmental conditions that increase (decrease) boundary-layer moisture could lead to more (fewer) open cell occurrences, affecting the albedo and cooling effect of the stratocumulus decks.

Another implication is that high amounts of aerosols could delay or suppress rain formation, and consequently closed-to-open cell transition (Rosenfeld et al., 2006; Yamaguchi et al., 2017; Goren et al., 2019). This suggests that the recent trend of decreasing aerosol amounts may lead to a positive forcing (i.e. warming) through earlier transitions from closed to open cells along their trajectories.

In contrast to the closed-to-open transition discussed here, it is thought that the transition from stratocumulus to cumulus is mainly driven by environmental factors (Wood, 2012; Eastman et al., 2022; Zheng and Miller, 2022; McCoy et al., 2023). More specifically, it is thought that the clouds drift over warmer sea surface temperatures, leading to deeper and decoupled boundary layers in which cumulus clouds form. However, the role of precipitation in this transition is still debated (Wood, 2012; Yamaguchi et al., 2017). The development of open cells as a mediating state may influence the timing of the stratocumulus-to-cumulus transition, and consequently the cloud albedo.

4.3 Uncertainties and robustness

Our mesoscale cloud typing is based on a CNN applied to GOES and MSI imagers, and uncertainties in these classifications propagate into both the inferred contrasts between open and closed cells and the estimated time-to-transition. Manual inspection suggests a failure mode is the potential misclassification of dissipating or fragmented cloud scenes as open cells, which would bias the retrieved LWP and RWP low for the open-cell category. Another difficulty lies in scenes with clouds that are at the edge of transitions or breaking up (see Fig. 10). Here, the CNN usually classifies scenes as closed cells if more than half of the scene is covered by them, and vice versa for open cells. Therefore, the cloud and rain properties around the transition time may be partially derived from the other cloud regime covering part of the scene.

Note also that neural networks trained on different regions, seasons, or cloud scene sizes can encode systematically different notions of “open” and “closed” cells. In our case, the fixed scene size of 128×128 km limits detectability of very large cell sizes and may preferentially capture smaller-scale open cells. This scale dependence should be considered when interpreting differences with prior work.

In addition to classification uncertainties, uncertainties in the EarthCARE retrievals must also be acknowledged. These products are still maturing, and forthcoming retrieval updates may affect some variables, particularly the distribution of cloud and rain particles within the vertical profiles. For this reason, we focus on column-integrated cloud and rain properties that are more robust and additionally constrained by the passive MSI imager.

Please note that our study focuses on daytime retrievals only, since the current version of the fine-tuned CNN only operates during the day. Cloud properties may exhibit diurnal cycles, which could impact transition processes (Pugsley et al., 2025).

https://doi.org/10.5194/egusphere-2026-3000
Preprint. Discussion started: 18 June 2026

However, this aspect is not addressed in our study. As mentioned above in Sect. 3.2, we observe a diurnal pattern in the number of transitions, with the majority occurring around dawn. Although the timing of transitions is more challenging at night, introducing an element of uncertainty into their distribution (see Sect. 2.6), this observation suggests that the diurnal cycle plays an important role in the transition process. A possible next step would be to incorporate night-time overpasses and study the effect of the diurnal cycle on closed and open cell properties and their transitions directly.

Further, the nature of active remote-sensing measurements may enhance the spread in our results. Depending on the exact satellite-ground track position relative to the mesoscale cloud structure, EarthCARE may sample different parts of the same cloud regime. In some cases, the satellite passes directly over the centres of cells or over regions of strong precipitation; in other cases – particularly for open-cellular scenes – it may sample mainly cloud edges or optically thinner areas. These geometric and structural differences naturally produce variability in the measured quantities. Such scene-dependent sampling differences are therefore expected to contribute to the overall dispersion in the data.

Finally, we would like to comment on the spread in many of the variables in the time series plots (Figs. 11, 12 and 13). This spread is often substantial relative to the magnitude of the detected trends. Therefore, one might argue that caution should be exercised when interpreting the observed trends. However, it should be noted that transition detection as well as time-to-transition estimation are performed independently for each cloud scene. The fact that smooth and coherent trends emerge despite this independence strengthens our confidence that the observed signals are physically meaningful.

4.4 Generality across regimes

Our analysis targets clouds in the subtropics and focuses on cloud and rain microphysics, since observations and theory suggest that the closed-to-open cell transitions are mainly driven by microphysical processes instead of large-scale meteorological conditions (Wood and Hartmann, 2006; Comstock et al., 2007; Bretherton et al., 2010; Berner et al., 2013; Glassmeier and Feingold, 2017; Smalley et al., 2022; Hoffmann et al., 2023). While we expect the microphysical processes as discussed in this work to hold in every situation, meteorological factors can still be of crucial importance in changing the initial cloud conditions or the timeline of transitions, for example by facilitating or hindering the development of rain. Eastman et al. (2022) found that increased wind speeds are associated with the development of open cells, which is consistent with our interpretation of increased moisture as a trigger for transitions. McCoy et al. (2017) and McCoy et al. (2023) found that a stronger instability, i.e. weaker boundary layer inversion strength, is associated with an increasing frequency of open cells. They show that this effect is strongest in mid and high latitudes, suggesting that the relative importance of precipitation feedbacks versus large-scale forcing is likely regime-dependent. Nevertheless, they still find a pronounced effect also in the subtropics. In future work it would be interesting to check the dependence of the transition timeline studied here on meteorological factors, like the inversion strength or sea surface temperature, to better understand how closed-to-open cell transitions might change in a changing climate.

https://doi.org/10.5194/egusphere-2026-3000
Preprint. Discussion started: 18 June 2026

5 Conclusions

This study utilizes the newly launched EarthCARE satellite to provide unprecedented insights into the properties of closed and open stratocumulus cells and the processes driving transitions between them.

EarthCARE has several advances compared to previous satellites that make it well suited to study low-level clouds. The combination of active (ATLID and CPR) and passive (MSI) sensors on the same platform enables simultaneous measurement of cloud mesoscale structure and detailed observations below cloud top. The CPR instrument is more sensitive than previous spaceborne radars, like CloudSat, and equipped with Doppler capabilities. This enables EarthCARE to overcome previous CloudSat limitations caused by ground clutter, better constrain rain and cloud retrievals and to detect even weak drizzle and small raindrops. Advanced retrieval techniques, like the optimal estimation algorithm of the ACM-CAP product, make use of the synergy of three instruments and are able to retrieve cloud and rain properties in unprecedented detail.

By applying a convolutional neural network to MSI data, we classify cloud mesoscale structures and analyse their microphysical properties using EarthCARE's synergistic measurements for a timespan of more than 15 months. Our results show that open cells differ markedly from closed cells especially in terms of microphysics. Open cells exhibit lower droplet number concentrations and more variable droplet sizes and liquid water paths. They have a higher frequency of rain occurrence, even though it should be noted that also closed cells rain in about 60 % of the cases. The larger difference is that open cells rain more heavily. They are notably more efficient at producing large rain amounts for a given liquid water path, primarily due to larger raindrop sizes.

To investigate the mechanisms behind closed-to-open cell transitions, we combine EarthCARE observations with GOES/ABI geostationary imagery and ERA5-driven wind trajectories. This approach allows us to track the evolution of cloud properties around closed-to-open cell transitions. We find that liquid water path and rain amounts in closed cells start to deviate from their climatological values up to 25 h before a transition, followed closely by a decrease in droplet number concentration and an increase of droplet sizes. The vertical cloud structure remains largely unchanged during this period.

Taken together, these findings support a precipitation-linked pathway to the closed-to-open transition, consistent with the cold pool convergence hypothesis presented by Feingold et al. (2010). The observed sequence is consistent with a feedback loop in which increased boundary-layer moisture enhances liquid water path and precipitation, leading to aerosol scavenging, reduced droplet number concentrations, and further precipitation intensification. An important point from the observed timeline is that the microphysical changes and gradual intensification of rain occur over a relatively long period of around 25 h before ultimately leading to a transition. This is consistent with previous work from Eastman et al. (2022), who find that closed-to-open cell transitions are preceded by strong winds and high latent heat flux for lead times of $\sim$3 days followed by microphysical cloud changes on timescales of 12–24 h.

We observe a pronounced diurnal cycle in the transition probability, with peaks occurring at dawn. This suggests that radiative cooling, leading to a gradual increase in cloud and rain water during the night, is an important part of the transition process, facilitating the formation of heavy rain necessary for open cell formation.

https://doi.org/10.5194/egusphere-2026-3000
Preprint. Discussion started: 18 June 2026

The new capabilities of EarthCARE enable high-sensitivity, fully collocated observations of cloud microphysics and precipitation, overcoming key limitations of previous satellite studies. A particular strength of this work is the synergy between these detailed EarthCARE retrievals and the high temporal resolution of GOES. This combination allows us to track the evolution of cloud properties around transitions with unprecedented detail, enabling the reconstruction of a physically coherent timeline of the microphysical processes governing closed-to-open cell transitions.

Nevertheless, several limitations should be acknowledged. Uncertainties arise from the CNN-based cloud classification, the use of ERA5-driven trajectories, and the EarthCARE retrievals, which, although advanced, are still maturing. The analysis is further limited to daytime conditions and subtropical regions. While robust temporal trends emerge across many transitions, the substantial variability indicates that additional factors, such as meteorological conditions, also influence the transition pathway.

Our results provide observational evidence that closed-to-open cell transitions are closely linked to precipitation-driven processes operating over timescales of about one day. This highlights the importance of representing aerosol-cloud-precipitation interactions in models to capture stratocumulus organization and its evolution. Because transitions from closed to open cells reduce cloud fraction and albedo, factors that modulate boundary-layer moisture or aerosol loading - such as changes in large-scale circulation or anthropogenic emissions - may strongly influence the radiative effect of marine stratocumulus.

Overall, this study demonstrates the power of EarthCARE's synergistic measurements for advancing our understanding of stratocumulus clouds and their controlling processes, and provides new observational constraints to improve the representation of stratocumulus clouds and their feedbacks in weather and climate models.

Code and data availability. The code and datasets used in this study, as well as the weights of the fine-tuned CNNs for MSI and GOES, can be found and downloaded via the EarthCODE platform: https://opensciencedata.esa.int/products/earthcare-marine-stratocumulus-transitions/collection.

Video supplement. An animation of the tracking of cloud structures using a combination of ERA-5 wind trajectories and the CNN applied to GOES (corresponding to the example shown in Fig. 4) can be found on the AV Portal of TIB Hannover.

Appendix A: Fine-tuning of the CNN

To adapt the CNN of Wu et al. (2025) to MSI and GOES imagery, we fine-tune the model using manually labeled cloud scenes. In total, 533 MSI scenes and 479 GOES scenes are labeled according to the six mesoscale structure classes (solid stratus, closed MCC, open MCC, disorganized MCC, clustered cumulus, and suppressed cumulus). For MSI, the labeled scenes are randomly drawn across all times and all four subtropical stratocumulus regions (SEP, NEP, SEA, and NEA), whereas GOES labels are drawn from the SEP region. Because of the natural variability of the occurrence of the different mesoscale structures, some structures are sampled more often than others (see Table A1), with closed cells being the most frequent cloud structure. Fine-tuning is applied only to the final network layer and performed using the `torch.optim.Adam` optimizer. To identify

https://doi.org/10.5194/egusphere-2026-3000
Preprint. Discussion started: 18 June 2026

Table A1. Number of manually labeled cloud scenes for MSI and GOES per mesoscale cloud structure class. The number of scenes withheld from traning and used for evaluation is displayed in parenthesis.

Class	number of scenes (used for evaluation)	
	MSI	GOES
Solid stratus	49 (16)	23 (5)
Closed MCC	150 (50)	183 (37)
Open MCC	64 (21)	81 (16)
Disorganized MCC	75 (25)	95 (19)
Clustered Cu	124 (41)	61 (12)
Suppressed Cu	71 (23)	36 (7)
Overall	533 (176)	479 (96)

Table A2. Overall classification performance for MSI on the validation dataset (176 scenes) for the CNN fine-tuned to MSI and the original CNN. Overall accuracy is the average accuracy over all cloud structure classes; equally-weighted accuracy takes into account that the classes have different numbers of samples.

Metric	Fine-tuned	Original
Overall accuracy (%)	86.36	72.73
Equal-weighted accuracy (%)	84.91	71.73

an optimal fine-tuning configuration, we conduct a hyperparameter grid search over learning rate, batch size, and number of epochs (learning_rate $\in 5\times10^{-5}$, 10^{-4}, 5×10^{-4}, batch_size $\in$ 4, 8, 16, num_epochs $\in$ 15, 20, 30). Part of the labeled dataset is withheld from training and used exclusively to evaluate model performance (see Table A1).

A1 Evaluation of the fine-tuned CNN for MSI

Performance is quantified for both the fine-tuned and the original model to get an estimate of the models improvement due to fine-tuning. The confusion matrix in Fig. A1 shows how the performance of the CNN changes after fine-tuning: Most of the cloud structure classes have a higher accuracy, especially open-cell detection is strongly improved. Table A2 shows the average performance of the models over all cloud classes, using two different methods of averaging. It shows that the average performance is improved for the fine-tuned model by about 13 to 14%. Since our analysis focuses on stratocumulus mesoscale cellular convection, we emphasize performance for the closed- and open-MCC classes, which both show improvements in precision and recall. This can be quantified in the F1 score: closed cells have an F1 score of 0.86 in the fine-tuned and 0.76 in the original model; open cells have an F1 score of 0.9 in the fine-tuned and 0.5 in the original model. Overall, fine-tuning substantially improves MSI classification performance, most notably for open MCC, where both per-class accuracy and F1 score increase markedly relative to the original model.

https://doi.org/10.5194/egusphere-2026-3000
Preprint. Discussion started: 18 June 2026

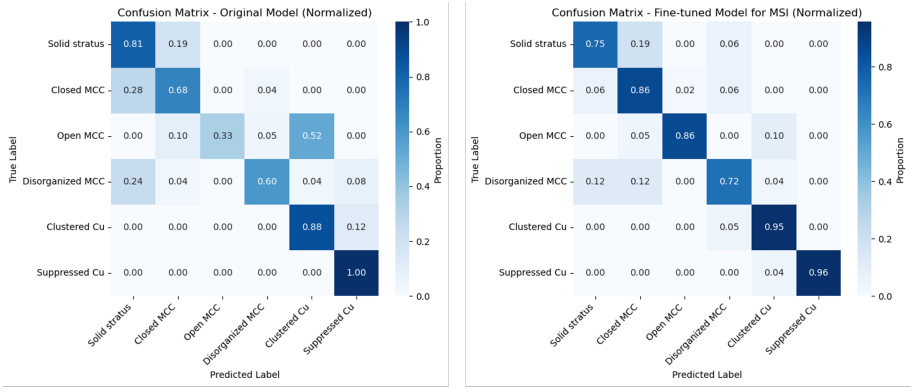

Figure A1. Confusion matrix for the performance of original CNN applied to MSI, and the CNN fine-tuned to MSI applied to the same scenes.

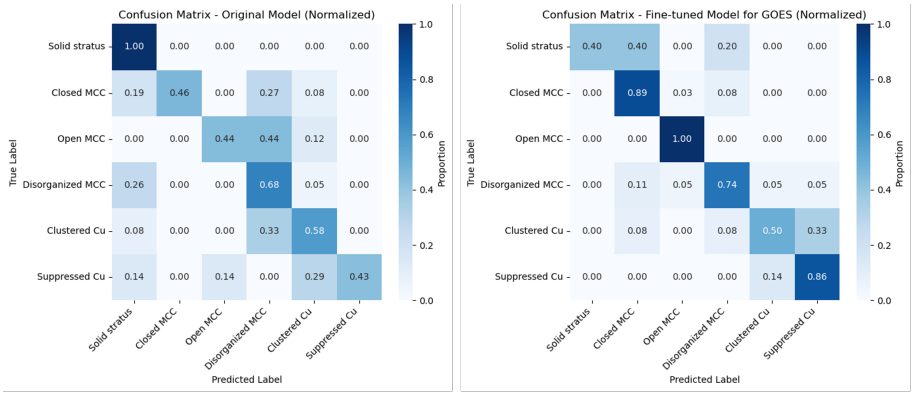

Figure A2. Confusion matrix for the performance of original CNN applied to GOES, and the CNN fine-tuned to GOES applied to the same scenes.

A2 Evaluation of the fine-tuned CNN for GOES

We evaluate the GOES fine-tuned CNN analogously. Performance is summarized using the same metrics as for MSI, and we again compare against the original model evaluated on the identical validation dataset. Per-class accuracy is strongly improved, especially also for closed and open cells (see Fig. A2). The solid stratus class shows worse performance after fine-tuning, however, in the manually labeled dataset for GOES there were only very few samples of this class (see Table A1), and the evaluation is therefore more uncertain than for other cloud structure classes. The average performance shown in Table A3 shows a strong average improvement for the fine-tuned model between 13 and 26%, depending on which measure is used. The F1 scores for closed cells are 0.88 for the fine-tuned and 0.63 for the original model; the F1 scores for open cells are 0.94 for the fine-tuned and 0.58 for the original model, showing that the balance of precision and recall is highly improved after fine-tuning.

https://doi.org/10.5194/egusphere-2026-3000
Preprint. Discussion started: 18 June 2026

Table A3. As Table A2, but for GOES.

Metric	Fine-tuned	Original
Overall accuracy (%)	80.21	54.17
Equal-weighted accuracy (%)	73.10	59.88

Appendix B: Properties of closed and open cells - percentiles

As a complement to Fig. 8, this figure illustrates additional aspects of the distributions of cloud and precipitation properties for closed and open cells. Shown are the 25th percentile, median, and 75th percentile for each variable, computed over 128 km cloud scenes using ACM-CAP retrievals. These percentile-based statistics highlight differences in distribution shape and variability that are not fully captured by the mean and CV alone.

Appendix C: Examples of transitioning cloud scenes

To illustrate the time evolution in cloud and rain properties around closed-to-open cell transitions, we show M-COP LWP, ACM-CAP LWC and RWC, and CPR reflectivity for example scenes for each time-to-transition value.

Author contributions. Conceptualization, formal analysis, software and writing of the original draft was done by JM. Development of the methodology and research questions was done by JM with very valuable help from BPG, EM and DG. SM and RH developed the ACM-CAP product and provided, besides data, valuable insights into the product and its interpretation. All authors contributed to reviewing and editing of the manuscript.

Competing interests. The authors declare no competing interests.

Acknowledgements. Thanks to the ESA/ESRIN Science Hub for providing the opportunity to conduct this research. Artificial Intelligence tools (DeepL, ChatGPT) were used for language editing of the manuscript. GitHub Copilot was used to assist in coding tasks.

https://doi.org/10.5194/egusphere-2026-3000
Preprint. Discussion started: 18 June 2026

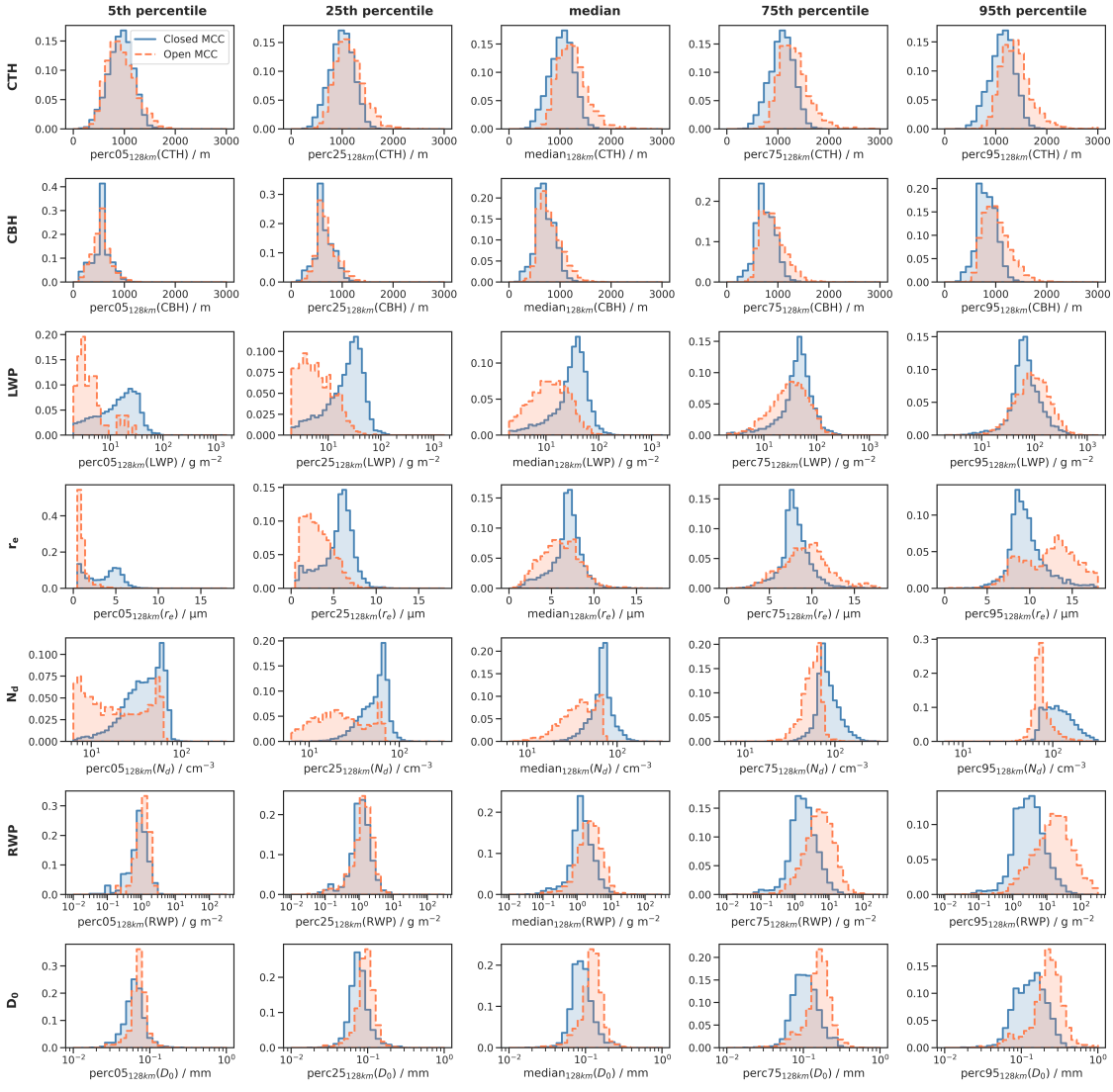

Figure B1. Same as Fig. 8, but for percentiles and median per cloud scene.

https://doi.org/10.5194/egusphere-2026-3000
Preprint. Discussion started: 18 June 2026

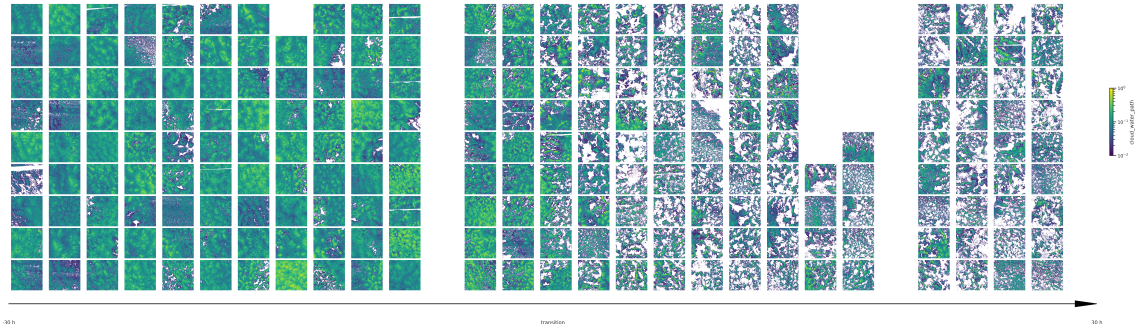

Figure C1. M-COP LWP for example cloud scenes for which closed-to-open cell transitions were identified. The scenes are ordered from left to right by their time to transition, using the same time-to-transition bins as in Figs. 11, 12 and 13. For each time to transition value, nine scenes were picked randomly. For some time-to-transition values less than nine scenes were found overall, and for time-to-transitions $= -5$ h and 19 h no corresponding scenes were found (see Fig. 11(a)).

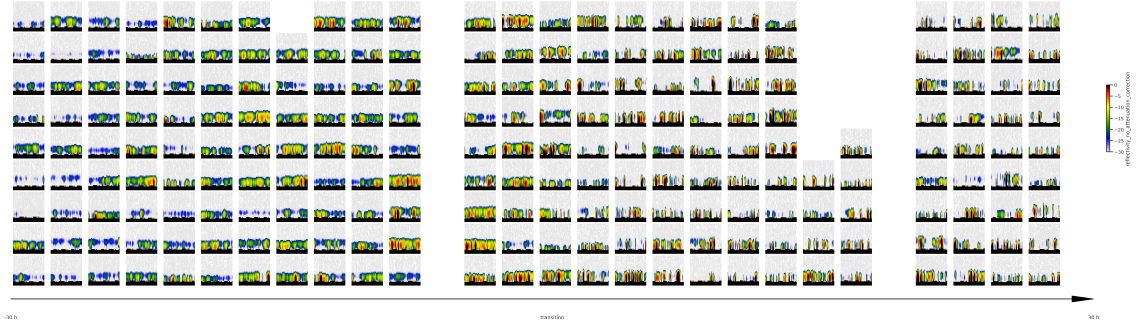

Figure C2. Same as Fig. C1, but for CPR reflectivity. The scenes correspond to the ones shown in Fig. C1.

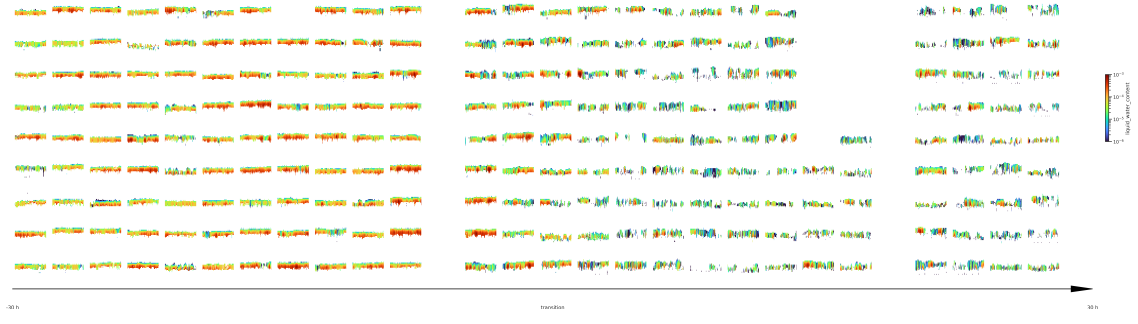

Figure C3. Same as Fig. C1, but for ACM-CAP liquid water content. The scenes correspond to the ones shown in Fig. C1.

https://doi.org/10.5194/egusphere-2026-3000
Preprint. Discussion started: 18 June 2026

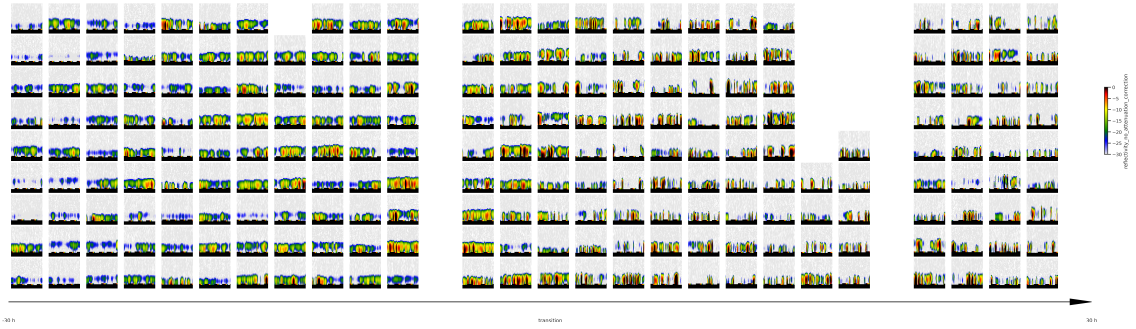

Figure C4. Same as Fig. C1, but for ACM-CAP rain water content. The scenes correspond to the ones shown in Fig. C1.

References

Berner, A. H., Bretherton, C. S., Wood, R., and Muhlbauer, A.: Marine boundary layer cloud regimes and POC formation in a CRM coupled to a bulk aerosol scheme, Atmospheric Chemistry and Physics, 13, 12 549–12 572, https://doi.org/10.5194/acp-13-12549-2013, 2013.

Bony, S. and Dufresne, J.: Marine boundary layer clouds at the heart of tropical cloud feedback uncertainties in climate models, Geophysical Research Letters, 32, https://doi.org/10.1029/2005GL023851, 2005.

Bretherton, C. S., Uchida, J., and Blossey, P. N.: Slow Manifolds and Multiple Equilibria in Stratocumulus-Capped Boundary Layers, Journal of Advances in Modeling Earth Systems, 2, https://doi.org/10.3894/JAMES.2010.2.14, 2010.

Cadeddu, M. P., Ghate, V. P., and Mech, M.: Ground-based observations of cloud and drizzle liquid water path in stratocumulus clouds, Atmospheric Measurement Techniques, 13, 1485–1499, https://doi.org/10.5194/amt-13-1485-2020, 2020.

Ceppi, P., Brient, F., Zelinka, M. D., and Hartmann, D. L.: Cloud feedback mechanisms and their representation in global climate models, WIREs Climate Change, 8, https://doi.org/10.1002/wcc.465, 2017.

Chandrakar, K. K., Morrison, H., and Witte, M.: Evolution of Droplet Size Distributions During the Transition of an Ultraclean Stratocumulus Cloud System to Open Cell Structure: An LES Investigation Using Lagrangian Microphysics, Geophysical Research Letters, 49, https://doi.org/10.1029/2022GL100511, 2022.

Comstock, K. K., Yuter, S. E., Wood, R., and Bretherton, C. S.: The Three-Dimensional Structure and Kinematics of Drizzling Stratocumulus, Monthly Weather Review, 135, 3767–3784, https://doi.org/10.1175/2007MWR1944.1, 2007.

Danker, J., Sourdeval, O., McCoy, I. L., Wood, R., and Possner, A.: Exploring relations between cloud morphology, cloud phase, and cloud radiative properties in Southern Ocean's stratocumulus clouds, Atmospheric Chemistry and Physics, 22, 10 247–10 265, https://doi.org/10.5194/acp-22-10247-2022, 2022.

de Lozar, A. and Muessle, L.: Long-resident droplets at the stratocumulus top, Atmospheric Chemistry and Physics, 16, 6563–6576, https://doi.org/10.5194/acp-16-6563-2016, 2016.

Eastman, R., McCoy, I. L., and Wood, R.: Wind, Rain, and the Closed to Open Cell Transition in Subtropical Marine Stratocumulus, Journal of Geophysical Research: Atmospheres, 127, https://doi.org/10.1029/2022JD036795, 2022.

Eisinger, M., Marnas, F., Wallace, K., Kubota, T., Tomiyama, N., Ohno, Y., Tanaka, T., Tomita, E., Wehr, T., and Bernaerts, D.: The EarthCARE mission: science data processing chain overview, Atmospheric Measurement Techniques, 17, 839–862, https://doi.org/10.5194/amt-17-839-2024, 2024.

https://doi.org/10.5194/egusphere-2026-3000
Preprint. Discussion started: 18 June 2026

Feingold, G., Koren, I., Wang, H., Xue, H., and Brewer, W. A.: Precipitation-generated oscillations in open cellular cloud fields, Nature, 466, 849–852, https://doi.org/10.1038/nature09314, 2010.

Fons, E., Naumann, A. K., Neubauer, D., Lang, T., and Lohmann, U.: Investigating the sign of stratocumulus adjustments to aerosols in the ICON global storm-resolving model, Atmospheric Chemistry and Physics, 24, 8653–8675, https://doi.org/10.5194/acp-24-8653-2024, 2024.

Glassmeier, F. and Feingold, G.: Network approach to patterns in stratocumulus clouds, Proceedings of the National Academy of Sciences, 114, 10 578–10 583, https://doi.org/10.1073/pnas.1706495114, 2017.

Goren, T., Kazil, J., Hoffmann, F., Yamaguchi, T., and Feingold, G.: Anthropogenic Air Pollution Delays Marine Stratocumulus Breakup to Open Cells, Geophysical Research Letters, 46, 14 135–14 144, https://doi.org/10.1029/2019GL085412, 2019.

Group, G.-R. A. W.: NOAA Geostationary Operation Environmental Satellite-R Series (GOES-R Series) Advanced Baseline Imager (ABI) Level 2 Cloud and Moisture Imagery Products (CMIP)., https://doi.org/10.7289/V5736P36.

Hersbach, H., Bell, B., Berrisford, P., Hirahara, S., Horányi, A., Muñoz-Sabater, J., Nicolas, J., Peubey, C., Radu, R., Schepers, D., Simmons, A., Soci, C., Abdalla, S., Abellan, X., Balsamo, G., Bechtold, P., Biavati, G., Bidlot, J., Bonavita, M., Chiara, G. D., Dahlgren, P., Dee, D., Diamantakis, M., Dragani, R., Flemming, J., Forbes, R., Fuentes, M., Geer, A., Haimberger, L., Healy, S., Hogan, R. J., Hólm, E., Janisková, M., Keeley, S., Laloyaux, P., Lopez, P., Lupu, C., Radnoti, G., de Rosnay, P., Rozum, I., Vamborg, F., Villaume, S., and Thépaut, J.: The ERA5 global reanalysis, Quarterly Journal of the Royal Meteorological Society, 146, 1999–2049, https://doi.org/10.1002/qj.3803, 2020.

Hoffmann, F., Glassmeier, F., Yamaguchi, T., and Feingold, G.: On the Roles of Precipitation and Entrainment in Stratocumulus Transitions between Mesoscale States, Journal of the Atmospheric Sciences, 80, 2791–2803, https://doi.org/10.1175/JAS-D-22-0268.1, 2023.

Hünerbein, A., Bley, S., Deneke, H., Meirink, J. F., van Zadelhoff, G.-J., and Walther, A.: Cloud optical and physical properties retrieval from EarthCARE multi-spectral imager: the M-COP products, Atmospheric Measurement Techniques, 17, 261–276, https://doi.org/10.5194/amt-17-261-2024, 2024.

Jensen, M. P., Ghate, V. P., Wang, D., Apoznanski, D. K., Bartholomew, M. J., Giangrande, S. E., Johnson, K. L., and Thieman, M. M.: Contrasting characteristics of open- and closed-cellular stratocumulus cloud in the eastern North Atlantic, Atmospheric Chemistry and Physics, 21, 14 557–14 571, https://doi.org/10.5194/acp-21-14557-2021, 2021.

Koren, I., Tziperman, E., and Feingold, G.: Exploring the nonlinear cloud and rain equation, Chaos: An Interdisciplinary Journal of Nonlinear Science, 27, https://doi.org/10.1063/1.4973593, 2017.

Leon, D. C., Wang, Z., and Liu, D.: Climatology of drizzle in marine boundary layer clouds based on 1 year of data from CloudSat and Cloud-Aerosol Lidar and Infrared Pathfinder Satellite Observations (CALIPSO), Journal of Geophysical Research: Atmospheres, 113, https://doi.org/10.1029/2008JD009835, 2008.

Loeb, N. G., Ham, S.-H., Allan, R. P., Thorsen, T. J., Meyssignac, B., Kato, S., Johnson, G. C., and Lyman, J. M.: Observational Assessment of Changes in Earth's Energy Imbalance Since 2000, Surveys in Geophysics, 45, 1757–1783, https://doi.org/10.1007/s10712-024-09838-8, 2024.

Mantilla, J. D.: Python package 'backtrajectory-calculator', 2023.

Mason, S. L., Chiu, J. C., Hogan, R. J., and Tian, L.: Improved rain rate and drop size retrievals from airborne Doppler radar, Atmospheric Chemistry and Physics, 17, 11 567–11 589, https://doi.org/10.5194/acp-17-11567-2017, 2017.

Mason, S. L., Hogan, R. J., Bozzo, A., and Pounder, N. L.: A unified synergistic retrieval of clouds, aerosols, and precipitation from EarthCARE: the ACM-CAP product, Atmospheric Measurement Techniques, 16, 3459–3486, https://doi.org/10.5194/amt-16-3459-2023, 2023.

https://doi.org/10.5194/egusphere-2026-3000
Preprint. Discussion started: 18 June 2026

McCoy, I. L., Wood, R., and Fletcher, J. K.: Identifying Meteorological Controls on Open and Closed Mesoscale Cellular Convection Associated with Marine Cold Air Outbreaks, Journal of Geophysical Research: Atmospheres, 122, https://doi.org/10.1002/2017JD027031, 2017.

McCoy, I. L., McCoy, D. T., Wood, R., Zuidema, P., and Bender, F. A.: The Role of Mesoscale Cloud Morphology in the Shortwave Cloud Feedback, Geophysical Research Letters, 50, https://doi.org/10.1029/2022GL101042, 2023.

Mohrmann, J., Wood, R., Yuan, T., Song, H., Eastman, R., and Oreopoulos, L.: Identifying meteorological influences on marine low-cloud mesoscale morphology using satellite classifications, Atmospheric Chemistry and Physics, 21, 9629–9642, https://doi.org/10.5194/acp-21-9629-2021, 2021.

Muhlbauer, A., McCoy, I. L., and Wood, R.: Climatology of stratocumulus cloud morphologies: microphysical properties and radiative effects, Atmospheric Chemistry and Physics, 14, 6695–6716, https://doi.org/10.5194/acp-14-6695-2014, 2014.

Nakajima, T. and King, M. D.: Determination of the Optical Thickness and Effective Particle Radius of Clouds from Reflected Solar Radiation Measurements. Part I: Theory, Journal of the Atmospheric Sciences, 47, 1878–1893, https://doi.org/10.1175/1520-0469(1990)047<1878:DOTOTA>2.0.CO;2, 1990.

on Climate Change (IPCC), I. P.: Climate Change 2021 – The Physical Science Basis, Cambridge University Press, ISBN 9781009157896, https://doi.org/10.1017/9781009157896, 2023.

Petters, M. D., Snider, J. R., Stevens, B., Vali, G., Faloona, I., and Russell, L. M.: Accumulation mode aerosol, pockets of open cells, and particle nucleation in the remote subtropical Pacific marine boundary layer, Journal of Geophysical Research: Atmospheres, 111, https://doi.org/10.1029/2004JD005694, 2006.

Possner, A., Eastman, R., Bender, F., and Glassmeier, F.: Deconvolution of boundary layer depth and aerosol constraints on cloud water path in subtropical stratocumulus decks, Atmospheric Chemistry and Physics, 20, 3609–3621, https://doi.org/10.5194/acp-20-3609-2020, 2020.

Pugsley, G., Gryspeerdt, E., and Nair, V.: Cloud fraction response to aerosol driven by nighttime processes, Proceedings of the National Academy of Sciences, 122, https://doi.org/10.1073/pnas.2509949122, 2025.

Rosenfeld, D., Kaufman, Y. J., and Koren, I.: Switching cloud cover and dynamical regimes from open to closed Benard cells in response to the suppression of precipitation by aerosols, Atmospheric Chemistry and Physics, 6, 2503–2511, https://doi.org/10.5194/acp-6-2503-2006, 2006.

Savic-Jovcic, V. and Stevens, B.: The Structure and Mesoscale Organization of Precipitating Stratocumulus, Journal of the Atmospheric Sciences, 65, 1587–1605, https://doi.org/10.1175/2007JAS2456.1, 2008.

Schmit, T. J., Griffith, P., Gunshor, M. M., Daniels, J. M., Goodman, S. J., and Lebair, W. J.: A Closer Look at the ABI on the GOES-R Series, Bulletin of the American Meteorological Society, 98, 681–698, https://doi.org/10.1175/BAMS-D-15-00230.1, 2017.

Sharon, T. M., Albrecht, B. A., Jonsson, H. H., Minnis, P., Khaiyer, M. M., van Reken, T. M., Seinfeld, J., and Flagan, R.: Aerosol and Cloud Microphysical Characteristics of Rifts and Gradients in Maritime Stratocumulus Clouds, Journal of the Atmospheric Sciences, 63, 983–997, https://doi.org/10.1175/JAS3667.1, 2006.

Smalley, K. M., Lebsock, M. D., Eastman, R., Smalley, M., and Witte, M. K.: A Lagrangian analysis of pockets of open cells over the southeastern Pacific, Atmospheric Chemistry and Physics, 22, 8197–8219, https://doi.org/10.5194/acp-22-8197-2022, 2022.

Stevens, B., Vali, G., Comstock, K., Wood, R., van Zanten, M. C., Austin, P. H., Bretherton, C. S., and Lenschow, D. H.: Pockets of Open Cells and Drizzle in Marine Stratocumulus, Bulletin of the American Meteorological Society, 86, 51–58, https://doi.org/10.1175/BAMS-86-1-51, 2005.

https://doi.org/10.5194/egusphere-2026-3000
Preprint. Discussion started: 18 June 2026

Stohl, A.: Computation, accuracy and applications of trajectories—A review and bibliography, Atmospheric Environment, 32, 947–966, https://doi.org/10.1016/S1352-2310(97)00457-3, 1998.

Terai, C. R., Bretherton, C. S., Wood, R., and Painter, G.: Aircraft observations of aerosol, cloud, precipitation, and boundary layer properties in pockets of open cells over the southeast Pacific, Atmospheric Chemistry and Physics, 14, 8071–8088, https://doi.org/10.5194/acp-14-8071-2014, 2014.

Wang, H. and Feingold, G.: Modeling Mesoscale Cellular Structures and Drizzle in Marine Stratocumulus. Part I: Impact of Drizzle on the Formation and Evolution of Open Cells, Journal of the Atmospheric Sciences, 66, 3237–3256, https://doi.org/10.1175/2009JAS3022.1, 2009a.

Wang, H. and Feingold, G.: Modeling Mesoscale Cellular Structures and Drizzle in Marine Stratocumulus. Part II: The Microphysics and Dynamics of the Boundary Region between Open and Closed Cells, Journal of the Atmospheric Sciences, 66, 3257–3275, https://doi.org/10.1175/2009JAS3120.1, 2009b.

Watson-Parris, D., Sutherland, S. A., Christensen, M. W., Eastman, R., and Stier, P.: A Large-Scale Analysis of Pockets of Open Cells and Their Radiative Impact, Geophysical Research Letters, 48, https://doi.org/10.1029/2020GL092213, 2021.

Wood, R.: Stratocumulus clouds, https://doi.org/10.1175/MWR-D-11-00121.1, 2012.

Wood, R. and Hartmann, D. L.: Spatial Variability of Liquid Water Path in Marine Low Cloud: The Importance of Mesoscale Cellular Convection, Journal of Climate, 19, 1748–1764, https://doi.org/10.1175/JCLI3702.1, 2006.

Wood, R., Comstock, K. K., Bretherton, C. S., Cornish, C., Tomlinson, J., Collins, D. R., and Fairall, C.: Open cellular structure in marine stratocumulus sheets, Journal of Geophysical Research Atmospheres, 113, https://doi.org/10.1029/2007JD009371, 2008.

Wood, R., Bretherton, C. S., Leon, D., Clarke, A. D., Zuidema, P., Allen, G., and Coe, H.: An aircraft case study of the spatial transition from closed to open mesoscale cellular convection over the Southeast Pacific, Atmospheric Chemistry and Physics, 11, 2341–2370, https://doi.org/10.5194/acp-11-2341-2011, 2011.

Wu, Y., Liu, J., Zhu, Y., Zhang, Y., Cao, Y., Huang, K.-E., Zheng, B., Wang, Y., Li, Y., Wang, Q., Zhou, C., Liang, Y., Sun, J., Wang, M., and Rosenfeld, D.: A global classification dataset of daytime and nighttime marine low-cloud mesoscale morphology based on deep-learning methods, Earth System Science Data, 17, 3243–3258, https://doi.org/10.5194/essd-17-3243-2025, 2025.

Xu, Z., Kollias, P., Sasikumar, S., Battaglia, A., and Treserras, B. P.: EarthCARE Cloud Profiling Radar Observations of the Vertical Structure of Marine Stratocumulus Clouds, Atmospheric Chemistry and Physics, https://doi.org/10.5194/egusphere-2025-5421, 2025.

Yamaguchi, T. and Feingold, G.: On the relationship between open cellular convective cloud patterns and the spatial distribution of precipitation, Atmospheric Chemistry and Physics, 15, 1237–1251, https://doi.org/10.5194/acp-15-1237-2015, 2015.

Yamaguchi, T., Feingold, G., and Kazil, J.: Stratocumulus to Cumulus Transition by Drizzle, Journal of Advances in Modeling Earth Systems, 9, 2333–2349, https://doi.org/10.1002/2017MS001104, 2017.

Yuan, T., Song, H., Wood, R., Mohrmann, J., Meyer, K., Oreopoulos, L., and Platnick, S.: Applying deep learning to NASA MODIS data to create a community record of marine low-cloud mesoscale morphology, Atmospheric Measurement Techniques, 13, 6989–6997, https://doi.org/10.5194/amt-13-6989-2020, 2020.

Zheng, Q. and Miller, M. A.: Summertime Marine Boundary Layer Cloud, Thermodynamic, and Drizzle Morphology over the Eastern North Atlantic: A Four-Year Study, Journal of Climate, 35, 4805–4825, https://doi.org/10.1175/JCLI-D-21-0568.1, 2022.